# Thin film materials for Li-ion batteries made by atomic layer deposition


Knut Bjarne Gandrud

Nanostructures and Functional Materials
Department of Chemistry and
Center for Materials Science and Nanotechnology

Faculty of Mathematics and Natural Sciences

University of Oslo

A thesis submitted for the degree of
*Philosophiae Doctor (Ph. D.)*
2014 April

*Series of dissertations submitted to the*
*Faculty of Mathematics and Natural Sciences, University of Oslo*
*No. 1519*

ISSN 1501-7710



Cover: Inger Sandved Anfinsen.
Printed in Norway: AIT Oslo AS.

Produced in co-operation with Akademika Publishing.
The thesis is produced by Akademika Publishing merely in connection with the thesis defence. Kindly direct all inquiries regarding the thesis to the copyright holder or the unit which grants the doctorate.

**“Imagination is more important than knowledge. For knowledge is limited to all we now know and understand, while imagination embraces the entire world, and all there ever will be to know and understand.”**

— Albert Einstein

As once promised,
this thesis is dedicated to
my Father

**Ove Gandrud**
04.07.1948 – 16.12.2007

*Thank you for opening my eyes*
*to all the wonders in this world.*

# Preface

The work that has resulted in this Ph. D. thesis called "*Thin film materials for Li-ion batteries made by atomic layer deposition*" started in November 2009 and is now approaching an end in April 2014. It was carried out at the Centre for Materials Science and Nanotechnology, Department of Chemistry, Faculty of Mathematics and Natural Sciences, Univeristy of Oslo, Norway. The financial support was received from the University of Oslo.

First, I would like to express my greatest gratitude to my supervisors, Professor Ola Nilsen and Professor Helmer Fjellvåg, for many valuable discussions and much appreciated help when writing the papers.

I would also like to thank all my colleagues at NAFUMA for creating a nice working environment, cooking excellent soups, and generally making these years enjoyable. In particular, I would like to thank Per-Anders Hansen for four great years in our office. Thank you for the many interesting discussions and enjoyable fights with our toy-soldiers. I would also like to thank all my friends both here in Oslo and on the west coast of Norway for letting me get some much-needed time off, occasionally.

Words cannot express how grateful I am for the support and love I have received from my lovely wife, Plamena. You and Masha (our cat) help me keep the right perspective in life, and you always manage to lift my spirit. Without the two of you, this work would have been a lonely journey.

I would like to thank my family for being supportive and genuinely interested in what I have been doing for these past years. And last, but not least, a huge thank you goes out to my dear mother for always being there for me. In addition to that, without her financial support during the last final months, when I had no income myself, it would have been rather difficult to finalize this thesis. I will pay you back, I promise!

Oslo, April 2014

Knut Bjarne Gandrud

# Table of Contents

# 1 Introduction

The current thesis has focused on one small, but important component in lithium batteries – the cathode material. The concept has been stretched further to focus on synthesis and behaviour of such materials at the nm-scale. Information on this endeavour will be given in the text below, but before going into depth, I would like to mention that lithium batteries can be divided into to main groups, primary (single use) and secondary (rechargeable) batteries. This work has only focused on rechargeable lithium batteries which, for simplicity, will throughout this thesis be referred to as lithium batteries (Li-batteries). In addition, there exists many different lithium battery technologies (Li-ion, PLiON, etc.), which again for simplicity, will all just be addressed as lithium batteries. This will suffice as they all use lithium in one form or another, and details about the differences between these technologies will not be addressed in this thesis.

Finally, in accordance with the convention used in the lithium battery field, all voltages quoted hereafter are defined with respect to lithium ($Li^+/Li$), unless otherwise indicated.

## 1.1 Motivation and scope of this thesis

Lithium batteries are becoming more important in our modern way of living as the number of devices utilizing them continuously increases, and our daily lives are to a greater extent dependent on their performance. Of the competing battery technologies we have today, the rechargeable lithium

battery is fundamentally the best[1] providing the highest specific energy (Wh/kg) and energy densities (Wh/l), see *Figure 1-1*. Lithium batteries can be found in a huge size-range of applications, ranging from microchips, medical implants, to portable applications as mobile phones, laptops and power tools, to electric cars and even large ships. Being able to store energy efficiently for applications of all size-ranges is a critical aspect for the transition from a carbon based society into a society based on renewable energy. Lithium batteries are a promising candidate for making this transition possible[2].

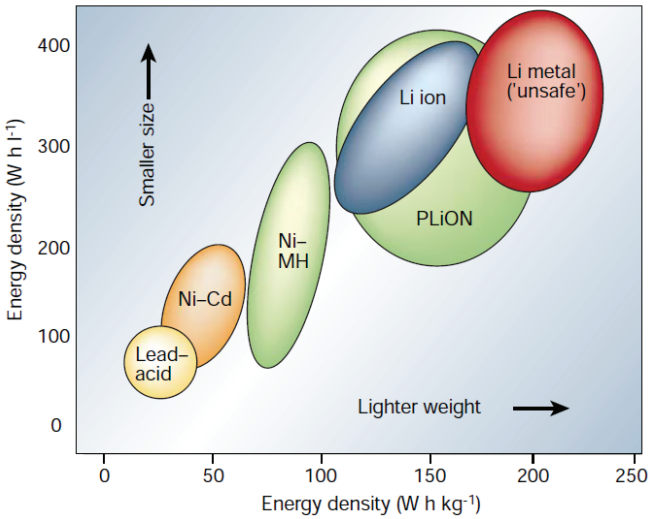


**Figure 1-1.** *A comparison of the specific energy (Wh/kg) and energy density (Wh/l) for lead-acid, nickel cadminum, nickel metal hydride, lithium-ion, lithium polymer (PLiON) and lithium metal secondary systems*[3].

Nevertheless, the demands of the lithium battery performances are increasing together with the growing number of applications and more

widespread usage. Ideally, a battery should practically last forever, be cheap, store vast amounts of energy, be able to both supply and receive energy quickly, be completely safe and also not contain any hazardous elements. Of course, you will not find a battery that is capable of all these feats, and there is still room for a lot of improvements in all of these areas in today's lithium batteries. In addition, with batteries it is as with most other cases in life; one can not simply have it all. An enhancement of the performance in one area (i.e. increased safety) often leads to poorer performance in other areas (power performance and price, for example). Naturally, a specific optimization of a battery is performed, depending on the application where it is going to be used.

Anyhow, the increased importance of lithium batteries in our daily life and in technological applications has resulted in intensive research and engineering efforts aimed at improving this technology. One can roughly divide the focus of battery research into three main areas: the anode, the electrolyte, and the cathode. Of these, the cathode materials play a critical role in terms of improving the cost, safety, power and energy densities of batteries. This is due to several factors, such as the cathode normally being the heaviest and most expensive component in a battery [4]. Furthermore, when compared to the carbon anodes we use today, the present cathode materials have around twice as low specific capacities[3, 5]. In many ways, this means that the development and improvement of cathode materials can be regarded as one of the major bottlenecks in the progress of developing better batteries. Of course, there is still room for a lot of improvements on both the anode side, and also regarding the electrolyte, however, in order to make cheaper and better batteries we really need better cathode materials.

Because of the critical role of cathode materials in battery development, they were chosen as the main focus for the work in this thesis with the challenging aim to develop improved cathodes for lithium batteries. We have used a technique called atomic layer deposition (ALD) for deposition of thin films of some selected battery cathode materials, with the aim to investigate the electrochemical properties of these thin film electrodes. Having the battery electrode as a thin film (<100 nm) has its advantages and drawbacks. Probably the main drawback is that the electrodes can store limited amounts of energy, so in order to make a practical battery (one that would be useful) we would need to utilize a high-surface area substrate to increase the total amount of energy the electrode can store. However, conformal deposition on complex surfaces and 3D-structures is one of the strengths of the ALD-technique [6]. To transfer the ALD processes used in this work, where we deposit on planar substrates, to 3-D substrates would likely require some optimization of the process parameters and might also require alternative precursor chemistries. Nevertheless, the main point is that the big drawback of the low energy density of thin film electrodes can be overcome.

One advantage of using thin films for investigation of electrochemical properties is that the small amount of active mass allows us to investigate ultra-high current rates[7]. As a quick example, if we have a 12 nm thick thin film electrode that has an active mass of only 7 μg (with the theoretical capacity of 178 mAh/g) we can run 3 mA through the battery which in this case would correspond to an ultra-high current rate of around 2500 C (I will explain C-rates more in detail later, but 2500 C corresponds to a 1.5s charge and discharge which is extremely fast for a battery!) Because only relatively small currents are used, heat generation inside the battery due to internal resistance is rather unproblematic. However, if we were to do the

same test with 70 mg of active material we would need to run 30 A through the battery, which would quickly result in the whole battery being destroyed due to heat generation from internal resistance (IR-losses) in the battery.

Nevertheless, the goals for this work have been to develop ALD processes to deposit thin films of the selected battery cathode materials $LiFePO_4$, $FePO_4$ and $V_2O_5$. Furthermore, as ALD enables precise thickness control of the deposited cathodes, we set out to obtain a better understanding for the electrochemical properties of these battery materials as a function of their thickness in the nm-range. By measuring the thickness dependent electrochemical properties both at low currents (thermodynamic equilibrium) and at ultra-high rates (kinetically limited), we believed we would obtain a good picture of their electrochemical properties. As materials also can "behave unexpectedly" when one or more of their dimensions approach the nm-level, there might be possibilities for discovering some new and surprising properties as well.

## 1.2 A brief history and future outlook

The concept of utilizing electrochemical reactions to do useful work may be far older than most people believe. Artefacts discovered in Iraq in 1936 suggest that batteries may have been used already as early as the year 250 BC[8]. Regardless the fact that batteries might have existed in the ancient world, today we consider the discovery of the battery to date from 1800, when Volta presented the first battery to the world. He called it the "voltaic pile", which was made of alternating plates of zinc and silver separated by cloth soaked in brine [9]. Since Voltas discovery several different chemistries and battery designs have seen the light of day[10],

however, the second big breakthrough in battery development happened in 1991 when Sony Corporation managed to pair a $LiCoO_2$ cathode (positive electrode) with a carbon (graphite) anode (negative electrode), to create and commercialize the first mass-produced rechargeable lithium battery[11]. Rechargeable batteries with a lithium metal anode and a Li-ion intercalation material (i.e. $TiS_2$[12]) as cathode was first demonstrated in the 1970s. Lithium had at that point long been considered a highly promising anode material, as it is the most electropositive material we have (giving rise to a high cell voltage) in addition to being the lightest metal (giving high energy densities). However, during recharging of these batteries, dendritic growth occurred as lithium ions were redeposited onto the lithium metal anode. Growth of these Li-metal dendrites would eventually penetrate the separator and electrolyte and reach the cathode, thus short-circuiting the connection between the electrodes, leading to thermal runaway with ensuing explosions and fires[13]. By exchanging the lithium metal anode with a graphite anode, that would intercalate Li-ions, Sony were able to produce a battery that had the benefits of a lithium metal anode, only with greatly improved safety and lifetime behaviour. This opened up for lithium batteries to become the dominant battery technology worldwide in the following years[14].

Indeed, there have been many improvements to the lithium battery after the initial launch by Sony. However, this progress have been rather slow, and if compared to the rate of progress in electronics (which follows Moore's law - doubling of capacity every two years), battery development are lagging behind. This is one area where 3D-structured thin film batteries might make a big impact,[15] by enabling energy storage devices that display high power capabilities while maintaining relative high energy densities. If we compare these 3D-structured electrodes to normal bulk electrodes, they will have a lower energy density. However, if we compare them to supercapacitors,

which have similar high power properties, they can store one to two orders of magnitude more energy[16].

Furthermore, there are several aspects with today's lithium batteries that can be improved upon. To quickly name a few: the capacity and voltage can be increased by finding new materials for the anode or cathode, solid-state-electrolytes can open up for new high-voltage chemistries, enhance the lifetime and safety, in addition to also enable more complex structured batteries. The electrochemical performance of existing anode and cathode materials can be improved upon by utilizing nanotechnology, conductive additives, surface modifications or doping. The battery field is without a doubt a challenging and exiting field to be working in, and I believe we will see a lot of improvements in the coming years.

## 1.3 Lithium batteries: A general introduction and some basic principles

A lithium battery normally consists of several cells that are connected in parallel or in series to obtain the desired voltage and capacity, however, in this work only single-cell systems have been used. As a consequence, the words battery and cell are used interchangeably in this thesis. A single-cell lithium battery consists of a positive and negative electrode, called the cathode and anode, respectively. Normally, the anode consists of some form of carbon, (i.e. graphite) and the cathode consists of a lithiated transition metal compound (i.e. $LiCoO_2$). The anode and cathode are kept apart by electrically insulating separator. In order to enable Li-ion transport between the two electrodes the separator is soaked in a liquid electrolyte, consisting

of a dissolved lithium salt (i.e. $LiPF_6$) in a mixture of organic alkyl carbonate solvents, such as ethylene, dimethyl, diethyl and ethyl methyl carbonate (i.e. EC, DMC, DEC, and EMC, respectively)[17]. Another important requirement of the liquid electrolyte is that it also must be electrically insulating, for avoiding short-circuiting of the cell. Once these electrodes are connected externally chemical reactions can proceed simultaneously at both electrodes, converting chemical energy to useful electrical energy, see *Figure 1-2*.

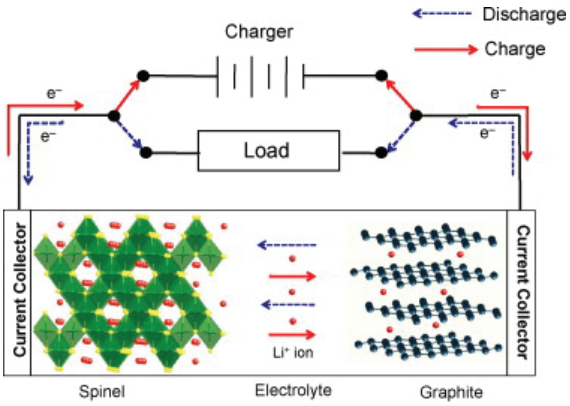


**Figure 1-2.** *A simple overview of a common lithium battery, illustrating the processes occurring during discharge and charge.*[18]

During discharge electrons leave the anode (it is oxidized) and travel to the cathode through the external circuit (doing useful work), while the lithium-ions are extracted (deintercalated) from the anode and travel to the cathode through the electrolyte. At the cathode, metal atoms in the host structure are reduced as they receive the electrons, and the lithium-ions traveling through the electrolyte are inserted into the cathode (intercalated). During charging the opposite reactions occur.

During discharge the driving force that causes electrons to move is the potential difference between the anode and cathode, called the cell voltage. We'll get back to this in more detail in the following theory chapter, but for now I will just simply say that the cell voltage is given by the difference in the chemical potential of lithium between the anode ($\mu$A) and the cathode ($\mu$C) [10, 19].

*Figure 1-3* shows a schematic energy diagram of a lithium battery at open-circuit. For the electrolyte the band gap $E_g$ between the lowest unoccupied molecular orbital (LUMO) and the highest occupied molecular orbital (HOMO) defines the stability window of the electrolyte. In order to have thermodynamic stability the redox energies of the anode ($\mu$A) and cathode ($\mu$C) must lie within this band gap. However, the redox energies of both lithium metal and graphite lie outside the stability window of the electrolytes used in today's lithium batteries. Luckily this is unproblematic because a solid electrolyte interfacial (SEI) layer is formed upon contact that prevents any further reactions from taking place between the electrolyte and anode.

A typical voltage range of the stability window for liquid electrolytes used in today's lithium batteries ($LiPF_6$ in EC:DMC) is between 1 to 4.5 V[1]. This stability window sets the limitations on the voltage of the chemistry used inside the battery, in addition it also sets the upper and lower limit in potential that the battery can be operated. For instance, if a given battery is charged above the upper stability limit of 4.5 V the electrolyte will start to decompose, which present a safety hazard and will in addition likely result in failure of the battery.

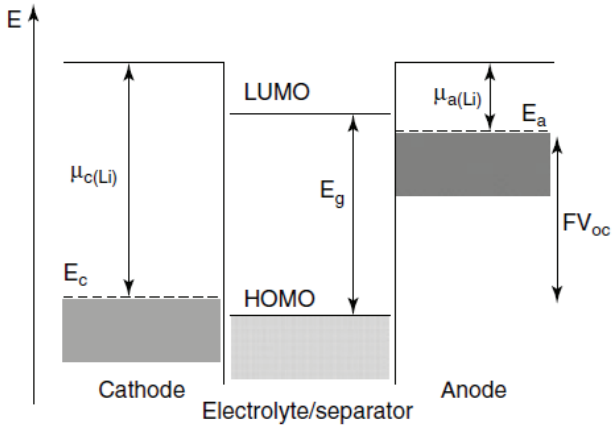


**Figure 1-3.** *Schematic energy diagram of a lithium battery at open circuit voltage. HOMO and LUMO refer to the Highest Occupied Molecular Orbital and the Lowest Unoccupied Molecular Orbital in the electrolyte, respectively*[10].

## 1.3.1 Specific capacity

The amount of electrical energy, expressed either per unit of weight (Wh/kg) or per unit of volume (Wh/l) that a battery is able to deliver is a function of the potential (V) and capacity (Ah/kg) both of which are linked directly to the chemistry of the system. The voltage is easy to compare between different systems as it is independent on the amount of material. However, when comparing capacities between two different materials, one often uses specific capacity (mAh/g). That is the amount of charge (in mAh) stored per gram of active material (the material that is participating in the redox reactions). This is an easy and simple way to compare the capacities of different electrode materials. However, one should keep in mind that for a real battery the capacity (per gram of battery) will be much lower than the

specific capacity of the electrode material, as you also need to factor in the weight of other components such as the casing of the battery, electrolyte and the other electrode.

### 1.3.2 C-rate and trade-off between power and energy

In order to help us to compare the electrochemical performance of different battery systems, we have something called C-rate. The reason we need these C-rates is due to the unfortunate fact that a battery behaves differently depending on how fast we want access to its stored energy. To put it simple, the faster we want the energy stored inside a battery to be released, the less energy we are going to get out. The same also applies for charging. This unfortunate behaviour is linked to kinetic limitations in the battery, and will be dealt with in more detail in the theory chapter. However, a typical way to display the trade-off between specific power and specific energy for different energy storage systems is with what is called a Ragone plot, see *Figure 1-4*.

Now that we know a bit more why C-rates are useful, let's see what a C-rate means: An *n*C-rate corresponds to a current that will completely charge or discharge the battery in 1/n hours. Thus, 1C corresponds to a current that will charge or discharge the battery in 1 hour, in the same manner C/10 and 1000C corresponds to a full charge or discharge in 10 hours and 3.6 second, respectively.

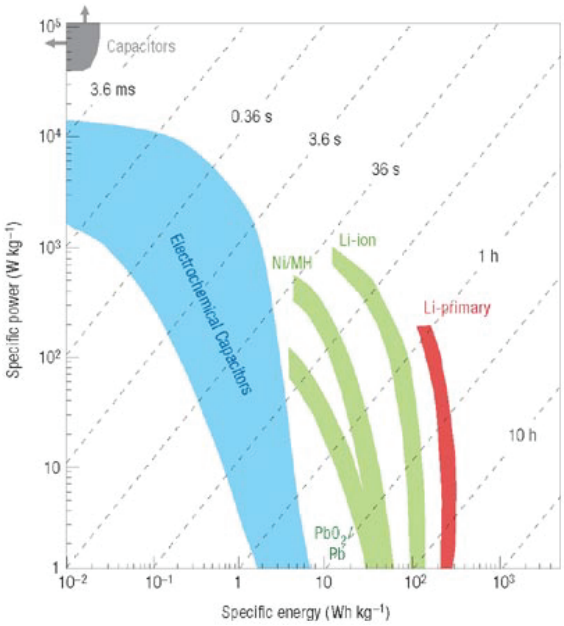


**Figure 1-4.** *A Ragone plot for various energy storage systems*[20].

## 1.4 The lithium battery cathode materials: $LiFePO_4$, $FePO_4$ and $V_2O_5$

As touched upon earlier, development of better cathodes is crucial for progress in the battery field. This chapter will give an introduction to the most central cathode materials studied in this work; crystalline olivine-type $LiFePO_4$ and the unlithated amorphous $FePO_4$, and a brief introduction of the cathode material $V_2O_5$.

## 1.4.1 $LiFePO_4$

The crystalline $LiFePO_4$ has been extensively studied in the literature, while amorphous $FePO_4$ (a-$FePO_4$) has received significantly less attention[21]. Most of the work done in this thesis focuses on the properties of amorphous $FePO_4$. However, as an introduction to these two materials let's first take a closer look on the well-known crystalline $LiFePO_4$, before coming back to the amorphous $FePO_4$.

Crystalline olivine-type $LiFePO_4$ (triphylite) was introduced to the world as a battery cathode material by Prof. Goodenoughs group in 1997[22]. As mentioned earlier, $LiCoO_2$ had been the cathode material of choice when Sony first introduced the rechargeable lithium battery in 1991, and since then it has been the most widespread used active material in conventional cathodes for lithium batteries[19]. However, this cathode material has some major drawbacks that are directly related to the nature of its chemical bonding. The d-states corresponding to the $Co^{3+/4+}$ redox couple are pinned at the top of the O 2p band [2b], see *Figure 1-5*. This has the unfortunate consequence that before all the electrons can be removed from these Co d-states, which occurs during charging of the battery, electrons are instead removed from the oxygen 2p-states. If this happens the cathode material itself decomposes, resulting in production of oxygen gas inside the battery, which needless to say poses a great safety hazard. The result of this is that only half of the electrons can be removed from the Co d-states in $LiCoO_2$, meaning that the battery can only be charged up to the maximum value of $Li_{0.5}CoO_2$, that is reached at 4.0 V [2b]. This also limits the practical capacity (137 mAh/g) of this material to only half of the theoretical capacity (274 mAh/g). Furthermore, Co is both a toxic and an expensive material (due to limited availability)[23].

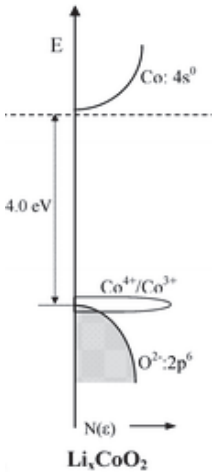


**Figure 1-5.** *Schematic of energy vs. the density of states for $LiCoO_2$ showing the pinning of the $Co^{3+/4+}$ redox couple at the top of the O 2p band [2b].The stippled line corresponds to the position of the $Li/Li^+$ redox couple.*

There has been an extensive effort to exchange Co with a less expensive and non-toxic element. Iron (Fe) was a promising candidate that is both abundant and non-toxic. However, by simply exchanging Co with Fe, the voltage obtained dropped considerably from 3.7 to 2.5V, due to the lower-valent redox couple that is $Fe^{2+/3+}$. Such a large voltage drop significantly lowers the amount of energy the battery can store. However, Prof. Goodenoughs group found a solution, which was to go from pure oxides into compounds consisting of polyanions $XO_4^{n-}$ (X = Mo, P and S). The effect of these polyanions is that the chemical bonding between the transition metal atom and the oxygen becomes weaker than in a pure oxide. If we choose Fe as the transition metal atom of interest, the redox energies of the $Fe^{2+/3+}$ couple will change in the compounds $Fe_x(XO_4)_y$ depending on the bonding in the $(XO_4)^{n-}$ polyanion in the following manner: The stronger

the X-O bonding the weaker the Fe-O bonding, and consequently the lower the $Fe^{2+/3+}$ redox energy relative to that in a simple oxide[10], see *Figure 1-6*.

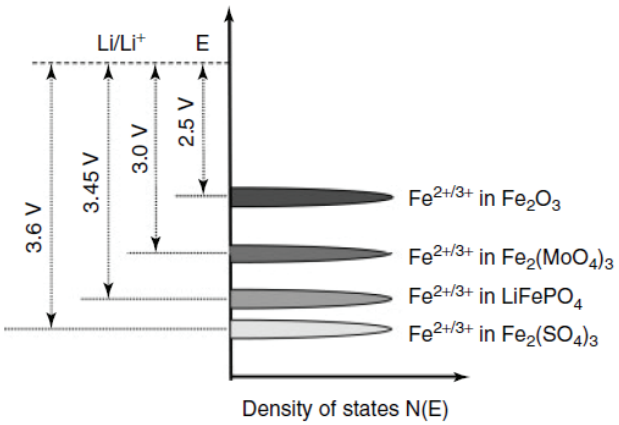


**Figure 1-6.** *Position of the $Fe^{2+/3+}$ redox energies relative to that of $Li/Li^+$ in various Fe-containing battery cathodes, and consequent changes in cell voltages illustrating the role of different polyanions[10].*

$LiFePO_4$ has the ordered-olivine structure with the space group *Pnma*. The crystal structure in *Figure 1-7* shows that the framework of this material consists of $FeO_6$ octahedra and $PO_4$ tetrahedra. Each $FeO_6$ octahedron is linked with four $FeO_6$ octahedra through common corners in the *b-c* plane, forming zigzag planes. These Fe-O planes are further interconnected by bridging $PO_4$ tetrahedra. The delithiated phase heterosite $FePO_4$ has essentially the same structure as $LiFePO_4$ but the $FePO_4$ host framework deforms slightly to an orthorhombic symmetry[23]. The structural similarity between $LiFePO_4$ and $FePO_4$ result in a volume decrease of only 6.81% when lithium is extracted from the structure[23], resulting in excellent

stability of the host structure and thus excellent lifetime behaviour during battery cycling.

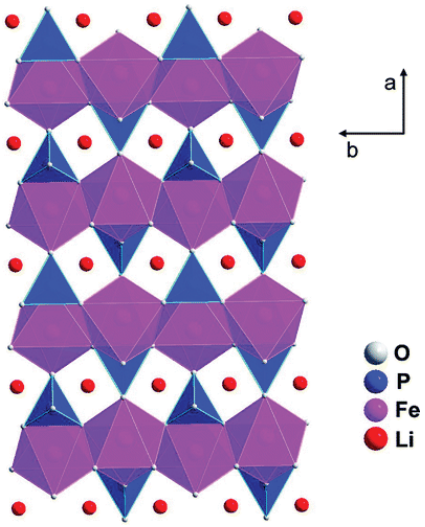


***Figure 1-7.*** *Structure of olivine $LiFePO_4$ (triphylite).*[23]

Since its identification as a potential cathode, $LiFePO_4$ has been the subject of extensive studies from both scientific and technological points of view. However, today, and more than 2000 research publications later, the electrochemical properties of this material is still not completely understood[24]. In the initial work, even at very low current densities, only 0.7 lithium ions were extracted per formula unit of $LiFePO_4$, which corresponds to a reversible capacity of < 120 mAh/g[22] (the theoretical capacity of this compound is 170 mAh/g). It was found that the lithium extraction/insertion occurred via a two-phase mechanism, resulting in flat plateaus on dis/charge profiles around ~3.45 V, with $LiFePO_4$ and $FePO_4$ as end members without much solid solubility[22, 24]. The low capacity was

attributed to the inherent poor electronic conductivity of this material ($10^{-7}$ – $10^{-9}$ S/cm for the lithiated phase[25] and ~$10^{-11}$ S/cm for the delithiated phase[26]) and also due to diffusion-limited transfer of lithium across the two-phase interface.

As researchers recognized that the poor reversible capacity and low rate capability might be linked to the poor electronic conductivity, a lot of effort went into increasing the electronic conductivity by coating the $LiFePO_4$ powder with conductive carbon. However, conductive additives alone were not enough to optimize the electrochemical performance. $LiFePO_4$ is a one-dimensional lithium-ion conductor with the lithium ion diffusion occurring along the b-axis, see *Figure 1-8*. The diffusion is rapid along these 1-D channels (~$10^{-8}$ to $10^{-9}$ $cm^2/s$ at room temperature) and negligible along perpendicular directions[24]. These channels are easily blocked by the most common point defect found in $LiFePO_4$ (Li-Fe anti-site) which involves $Fe^{2+}$ residing directly in the fast 1-D diffusion paths, blocking Li migration in the respective channel[27]. These Fe anti-site defects can thus render parts of the material inactive, thus both small particle sizes (~100 to 150 nm) and conductive additives were needed in order to obtain theoretical capacities[28].

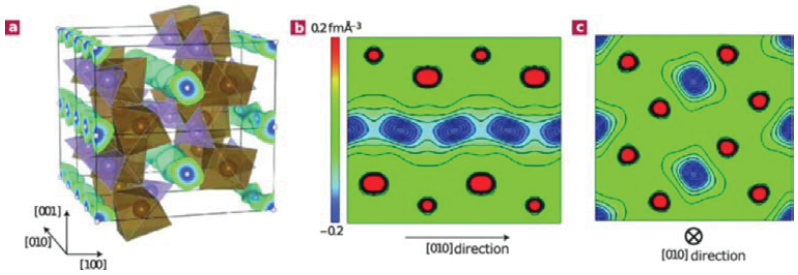


**Figure 1-8.** ***a)*** *Structure of* $LiFePO_4$ ***b)*** *and* ***c)*** *showing 1-D channels for lithium transport along the b-axis by measuring the Li nuclear density (blue contours)*[29].

Increasing the electrical conductivity of $LiFePO_4$ through doping with supervalent cations have also been tried. In 2002, Chiang and his colleagues claimed they raised the electronic conductivity of bulk $LiFePO_4$ by 8 orders of magnitude through low-level doping with the cations $Ti^{4+}$, $W^{6+}$ and $Nb^{5+}$[30]. This paper drew a surge of interest, and several cations were investigated as dopants, even multi-element doping and anion doping were carried out [23].

However, results obtained by Chiang and his colleagues are still under controversy, and it has later been shown that the observed increase in conductivity is likely not due to any doping effects, but rather due to surface conductive phases formed during the preparation process[31], or due to residual carbon from the carbonaceous precursors used[32]. In addition, theoretical studies have suggested that $LiFePO_4$ is not tolerant to aliovalent doping on either Li or Fe sites[33]. Thus, apart from the first report, there exists no convincing evidence for an increased rate capability due to aliovalent doping into bulk $LiFePO_4$ [23]. This leaves proper nanostructuring, which optimizes both the electrical contact and the Li solid-state diffusion

lengths, as one of the main tools for improving the electrochemical performance of this material. Finally, even though $LiFePO_4$ in bulk behave in a two-phase reaction mechanism during Li intercalation/deintercalation, a complete solid-solution behaviour has been observed for 40 nm sized nanoparticles[34]. This observation demonstrates how the electrochemical behaviour of a material can change radically once its dimensions are reduced to the nm-level.

Regarding the electrochemical performance of crystalline $LiFePO_4$, the best rate capability reported for this material is for a composite electrode consisting of 50 nm $LiFePO_4$ particles coated with a thin amorphous layer, that was further mixed with large amounts of carbon black (65 wt%) [16a]. This composite electrode could deliver 60 mAh/g at 400 C, meaning that 35 % of the theoretical capacity could be accessed during a 9 second discharge. Furthermore, at the highest tested rate of 400 C (68 000 A/kg) the specific power obtained from this electrode was 170 kW/kg (68 000 A/kg * 2.5 V). The observed specific power is similar to or higher than the specific power obtained from typical supercapacitors, however, with a specific energy that is one to two orders of magnitude higher. These findings suggest that the distinction between supercapacitors and batteries will blur out, as battery electrodes capable of extreme high rates are developed.

### 1.4.2 $FePO_4$

For the unlithiated material, $FePO_4$, there exists several modifications: orthorhombic $FePO_4$ (heterosite), which only can be obtained by delithiation of triphylite[26], monoclinic $FePO_4$, trigonal $FePO_4$ and amorphous $FePO_4$ (a-$FePO_4$). Of the crystalline phases, trigonal $FePO_4$ is the thermodynamic stable phase[26], and it is composed of $FeO_4$ and $PO_4$

tetrahedra, where each $FeO_4$ tetrahedron shares each of its four corners with four $PO_4$ tetrahedra, and vice versa, resulting in a quartz-like structure. However, the trigonal phase is almost completely electrochemically inactive as $Fe^{2+}$ is not stable in tetrahedral configuration[19], in addition it also has a much lower electronic conductivity (~$10^{-13}$ S/cm) then the heterosite phase[26]. The different modifications of $FePO_4$ have different electrochemical behaviour and the electrochemical activity decreases according to the order (from greatest to lowest):

a-$FePO_4$ > orthorhombic $FePO_4$ > monoclinic $FePO_4$ > trigonal $FePO_4$[23].

The amorphous counterpart to the crystalline $LiFePO_4$ has, as mentioned earlier, received much less attention from researchers worldwide[35]. It contains $FeO_6$ octahedra and $PO_4$ tetrahedra similar to the orthorhombic modification[36], however, its gravimetric density (~3.0 g/$cm^3$)[37] is closer to the trigonal phase (~3.0 g/$cm^3$) than the orthorhombic phase (~3.6 g/$cm^3$). The amorphous $FePO_4$ also shares the poor electronic conductivity of the olivine-type $LiFePO_4$, however, there are fewer reports on the exact values and these are also spread ranging from $10^{-6}$ to $10^{-8}$ S/cm [35, 37a]. In addition, the Li intercalation and deintercalation in amorphous $FePO_4$ show behaviour of a single-phase reaction[36], $Li_xFePO_4$, as opposed to the two-phase reactions shown by the orthorhombic modification[38]. This behaviour give rise to a sloping dis/charge profile, where lithium is extracted and inserted into the amorphous phase around ~3 V, [21, 36] with a theoretical capacity of 178 mAh/g. Furthermore, due to the amorphous nature of this material Li-ion diffusion can not be restricted by any defects [39], which as mentioned earlier, can be a problem for the olivine crystalline phase.

The highest rate performance reported for this material was for a hybrid electrode consisting of 10 to 20 nm particles of a-$FePO_4$ attached to a virus mixed with 5 wt% CNT (carbon nanotubes), and it showed a specific capacity of ~115 mAh/g at 10 C[40].

## 1.4.3 $V_2O_5$

Since, the first report in 1976 by Whittingham et al. where they reported that $V_2O_5$ can reversible intercalate lithium ions[41], this material has been intensively investigated as a cathode material for lithium batteries due to its low cost, abundance, and high energy density[42].

$V_2O_5$ has the orthorhombic crystal structure with the space group *Pmmn*[43]. It has a layered structure consisting of $V_2O_5$ layers packing along the c-axis, linked together by weak vanadium-oxygen interactions, and each layer is made of square pyramids of $VO_5$ sharing edges and corners[44], see *Figure 1-9*.

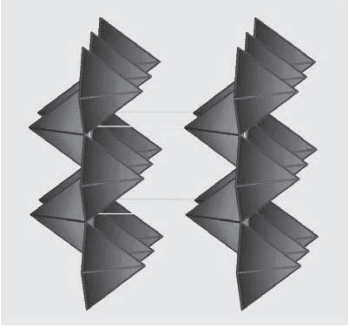

**Figure 1-9.** *Structure of $V_2O_5$ showing the square pyramids sharing edges of the basal plane.*[19]

Intercalating lithium into $V_2O_5$ is a rather complex process, if we for the following consider the formula:

$$Li_xV_2O_5 \qquad (0 \leq x \leq 3) \qquad (1.1)$$

During the initial lithium insertion in this compound, the α-$LiV_2O_5$ phase is first formed[19] at $x < 0.01$. Then the ε-phase, with increased puckering of the $V_2O_5$ layers, is formed[45] for $0.35 < x < 0.70$. At the $x = 1$, gliding of every other layer in the *b*-direction results in the δ-phase[45]. The transformations from $x = 0$ to $x = 1$ does not affect the strong V–O bonds and are fully reversible[45]. Intercalation of 1 mole of lithium per formula units of $V_2O_5$ corresponds to a theoretical capacity of 147 mAh/g.

An irreversible transformation to the γ-phase occurs at $x > 1$. Here the $V_2O_5$ layers are severely puckered, and some of the $VO_5$ pyramids changes orientation[19]. The above mentioned phase transitions are reflected in the discharge curve of $V_2O_5$ as three plateaus at 3.4, 3.2, and 2.3 V for the α/ε, ε/δ, and δ/γ two-phase regions, respectively[45].

Once the γ-phase is obtained it can be cycled reversible in the range $0 < x < 2$, corresponding to a theoretical capacity close to 300 mAh/g. However, this phase has slower kinetics due to lower Li diffusivity[45] , and it shows worse lifetime behaviour during cycling compared to the $x \leq 1$ phases[19, 45-46].

Upon further reduction below 1.9 V ($x > 2$) a tetragonal ω-$Li_3V_2O_5$ phase is formed[45], which upon further cycling quickly transforms into a disordered rock-salt structure[47]. The ω-phase can be cycled as a single solid-solution over the range $0 \leq x \leq 3$, corresponding to a theoretical capacity of 440

mAh/g[19]. However, it shows even slower kinetics and worse stability during cycling than the previous phases [19, 45-46].

The development of lithium batteries with $V_2O_5$ as the cathode has been limited because of poor structural stability[45], low electronic and ionic conductivities[48] and slow electrochemical kinetics[42]. In order to reduce the impact of poor electrochemical kinetics a lot of recent research has focused on the synthesis and fabrication of nanostructured vanadium oxides, giving high specific surface areas and short diffusion distances[49]. As our group recently have developed an ALD process[50] that yielded samples with a highly textured and nanostructured surface, consisting of crystalline $V_2O_5$ platelets, we wanted to study the electrochemical properties of these samples as a function of their thickness and morphology.

Regarding the electrochemical performance of $V_2O_5$, one of the best rate capability reported for this material is an electrode consisting of template based nanowires of $V_2O_5$[51]. When cycled in the potential range of 3.8 – 2.5 V this electrode could deliver 30 mAh/g at 1361 C (20% of the theoretical capacity for a 2.5s discharge), displaying an impressive specific power of ~500 kW/kg. They also observed that above 500 C the nanostructured electrode delivered four times the capacity of a 250 nm thin film control electrode, showing the importance of nanostructured electrodes for optimized high rate performance. However, the nanostructured electrode showed rather poor cycling stability (7% loss in capacity over 40 cycles).

# 2 Theory

This chapter presents the different theories and concepts utilized as a basis for evaluating and discussing the obtained results in this work. The focus will be on thermodynamic and kinetic aspects connected to lithium battery electrode materials, in addition to the electrochemical methods used to study said effects.

## 2.1 Rate limiting steps

For investigations of kinetic aspects, one can often simplify the prediction and analysis of behaviour by recognizing that a single reaction step may be much slower than all the others, thus controlling the rate of the overall reaction. This slowest reaction is often referred to as the rate-limiting step[52].

For intercalation of lithium ions into an electrode the possible rate-limiting steps can be summarised as follows (see, *Figure 2-1*):

1) Transport of lithium ions in the electrolyte towards the electrode surface.
2) Intercalation of lithium ions into the host structure, i.e. a charge transfer reaction.
3) Transport of lithium ions (i.e. diffusion) and electrons in the solid phase of the active electrode material.

Of these steps, the solid-state diffusion of Li-ions is considered to be the rate-limiting step in intercalation electrodes [18].

The mass-transport limitation of lithium ions in the liquid electrolyte (**Step 1**) is normally assumed to be insignificant and thereby neglected in the evaluation of the intercalation electrode kinetics. This approximation is generally motivated by the fact that the transport of lithium ions in the solid-state is significantly slower than in the liquid electrolyte.

In the continuation of this chapter we will go into more detail about the effects that can contribute to the kinetic aspects of the lithium intercalation reaction (i.e. **step 2** and **3**).

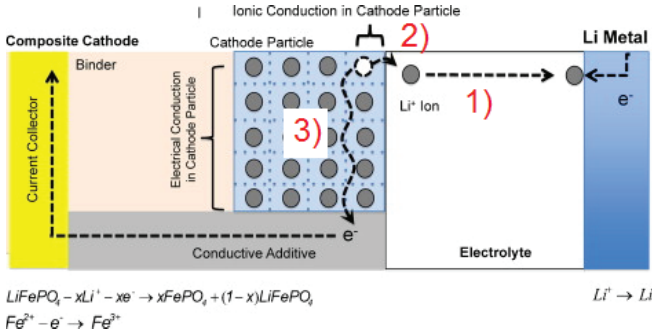


**Figure 2-1.** *Conduction phenomena in cathode particle ($LiFePO_4$) during charge.*[18]

In order to improve the kinetics, nanostructured electrode morphologies, such as nanoparticles, thin films, and others having at least one dimension at the nanometer level, have been considered. What normally can be expected from using a nanostructured electrode, which reduces the needed diffusion

length of lithium ions, are enhancements of the electrode charge and discharge rates [53].

However, it is of great importance in battery development to understand and distinguish between the rate-limiting processes that depend on the intrinsic properties of the material (e.g. solid-state diffusion and charge-transfer reactions) and the processes that are related to the preparation of the battery electrode (e.g. binders and conducting agents, particle size, and electrode porosity).

Interestingly, thin films with a precisely controlled thickness are ideal modelling systems for investigating the true rate-capability of electrode materials. Thin film electrodes contain no conductive additives or binders that can influence the measurements. In addition, all the parts of the active material have good and uniform electrical contact with the current collector, which often is not the case for many composite electrodes (active particles + conductive additives)[24].

## 2.2 Faraday's law and theoretical capacity

One of the most defining features of a lithium battery is its capacity, i.e. how much charge it can reversibly store. As mentioned in the introduction chapter, the capacity of a battery material (e.g. a cathode) is normally defined by its gravimetric or specific capacity, which is usually given in units of mAh/g. In order to calculate the theoretical capacity of a material, we need to be able to connect the total amount of charge measured from a reaction to the amount of material that reacted. Faraday's law lets us do this, and if we consider the simple half-reaction:

$$Ox + ne^- \rightarrow Red \qquad \textit{(Eq. 2-1)}$$

Then Faraday's law states that if $x$ moles of reagent Ox are reduced, the total amount of charge ($Q$) spent is given by[54]:

$$Q = nFx \qquad \textit{(Eq. 2-2)}$$

where, F is the Faraday constant (96485 C/mol), $n$ is the number of electrons needed per mole of Ox, and $Q$ is the said charge, given in coulombs ($C$).

An example calculation of the theoretical capacity of amorphous $FePO_4$ is shown below:

$$FePO_4 + xLi^+ + xe^- \leftrightarrow Li_xFePO_4 \qquad ,(\,0 \leq x \leq 1) \qquad \textit{(Eq. 2-3)}$$

During discharge, 1 mole of lithium is intercalated into 1 mole of $FePO_4$ resulting in the flow of 1 mole of electrons through the external circuit. Faraday's law (*Eq. 2-2*) then gives us that the total charge passed is:

$$Q = 1\,mol \times F \qquad \textit{(Eq. 2-4)}$$

The theoretical capacity $Q_T$ (C/g) is obtained by dividing the charge by the mass ($M_{FePO4}$) of the initial material (1 mol $FePO_4$ ~ 151 g):

$$Q_T = \frac{nF}{M_{FePO4}} \qquad \textit{(Eq. 2-5)}$$

*Eq. 2-5* gives the theoretical capacity in units of coulombs per gram (C/g). Converting the theoretical capacity from C/g to mAh/g (the more common measure of capacity) involves a simple conversion of charge from C (A/s) to mA/h, by dividing by 3.6. Thus for $FePO_4$ we get the theoretical capacity:

$$Q_T\left(\frac{mAh}{g}\right) = \frac{1mol \times 96485\ (\frac{C}{mol})}{151g \times 3.6} = 178\ mAh/g$$

## 2.3 Kinetic aspects for electrode reactions

The interface between the electrode material and the liquid electrolyte is a complex region in which, apart from the previously mentioned possibility of SEI-layer formation, several other effects do occur. The two most notably are the charge-transfer reaction and the electrostatic double-layer. The currents obtained from these two effects are termed Faradaic and non-Faradaic, respectively.

Faradaic current refers to a current generated from a reaction where there has been charge transfer across an interface (electrochemical reaction). For non-Faradaic currents no such charge-transfer occurs across an interface, the electrical energy is instead stored through electrostatic charge accumulation at the interface.

### 2.3.1 The Butler-Volmer equation

The Butler-Volmer is an important equation that relates the overpotential needed to pass a given current through an interface (charge-

transfer). This equation has not been used for any detailed analysis in this work, however, as it describes an important concept in batteries and it affects the kinetics, we'll quickly go through it here. For the details for obtaining this equation, see the book of P. Zanello[54].

If we consider the general electron-transfer process (taking place at the surface of an electrode):

$$Ox + ne^- \underset{k_{Ox}}{\overset{k_{Red}}{\rightleftharpoons}} Red \qquad \textit{(Eq. 2-6)}$$

The Butler-Volmer equations states that the current, *i,* is given as:

$$i = n\,F\,A\,k^0\left[C_{Ox}(0,t)e^{-\frac{\alpha\,n\,F}{R\,T}\eta} - C_{Red}(0,t)e^{\frac{(1-\alpha)\,n\,F}{R\,T}\eta}\right] \qquad \textit{(Eq. 2-7)}$$

Where:

*n* is the number of electrons transferred per molecule of Ox.

F is the Faraday constant.

*A* is the electrode area.

$k^0$ is the standard rate constant.

$C_{Ox}(0,t)$ and $C_{Red}(0,t)$ are the concentration of Ox and Red, respectively, at the electrode surface.

$\alpha$ transfer coefficient ($0 < \alpha < 1$).

R is the universal gas constant.

T is the temperature.

$\eta$ = surface overpotential ($E_{applied} - E_{equilibrium}$).

This equation relates the net current as the difference between the current generated from the reduction process (going one direction) and oxidation process (going the other direction). At equilibrium there is no net current, meaning that the current generated from the reduction and oxidation reactions cancel each other out. This current, equal in both directions and exchanged under equilibrium conditions, is defined as the exchange current, $i_0$. The exchange current is proportional to the standard rate constant for the electron-transfer process and a large $i_0$ indicates facile kinetics, which results in that smaller overpotentials are needed for a given current. The resulting current-overvoltage profile is shown in *Figure 2-2*.

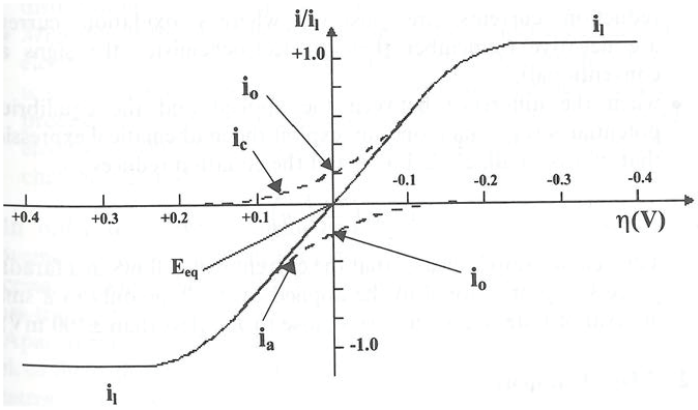


**Figure 2-2.** *Current-overpotential profiles for the process Ox + ne⁻ ↔ Red. Experimental conditions: α = 0.5; n = 1; T = 25°C. The current is normalized with respect to the limiting value $i_l$.*[54]

As can be seen from *Figure 2-2*, at negative overpotentials the anodic component (oxidation) is zero, so the current is only due to the reduction process. Naturally, at positive potentials the opposite is true, where the current is only due to the oxidation process. At high overvoltages the current

reaches a limiting value ($i_l$) beyond which it can rise no more. This happens when the current is no longer controlled by rate of the electron-transfer, but rather is limited by the rate of mass transport of the species Ox or Red. For a lithium battery electrode this would correspond to the current being limited by $Li^+$ diffusion[52].

## 2.3.2 The electrostatic double-layer

When a voltage is applied, an electric field develops across the interface and current flows until a given amount of charge builds up. The amount of charge stored ($Q$) is given by:

$$Q = C_{dl}V \qquad \textit{(Eq. 2-8)}$$

where, $C_{dl}$ is the capacitance of the double-layer, measured in Farads (Coulombs/Voltage). Furthermore, the current and voltage is related by[55]:

$$i = C_{dl}\,\frac{dV}{dt} \qquad \textit{(Eq. 2-9)}$$

In other words, the interface between the electrolyte and electrode behaves like a capacitor. However, unlike real capacitors, whose capacitances are independent of the voltage across them, $C_{dl}$ is often a function of potential[55]. The non-Faradaic currents can interfere with measurements of kinetic and transport properties, however, on the positive side it does also store energy. The charge is stored electrostatically, and therefore the amount of charge stored per electrode surface area is low, and usual values are 10 – 40 μF/cm$^2$.[56] In order to get a feeling on how much charge will be stored in this double layer, lets assume the highest capacitance value of 40 μF/cm$^2$

and that it is independent on the applied potential. For a typical electrode used in this work with a surface area of roughly 2 $cm^2$, the amount of charge stored would be maximum 80 μF, which corresponds to 80 μC/V. During a measurement where the voltage is varied over a potential window of 2 V, this would then result in 160 μC being stored electrostatically in the double-layer. If we compare this to a thin electrode of say 23 nm $FePO_4$ (we assume a density of 3.0 $g/cm^3$) with the same surface area, this material stores:

$$23 \times 10^{-7} cm \times 2\ cm^2\ \times 3.0 \frac{g}{cm^3} \times 178 \frac{mAh}{g} = 2.5\ \mu Ah \times 3600 = 9\ mC$$

This means that the amount of charge stored from the $Li^+$ intercalation reaction is ~55 times larger than what is stored in the electrostatic double-layer. In addition, as the capacitive current is proportional to the rate of change in the potential (i.e. dV/dt), the effect can be ignored if the electrochemical measurement is carried out at equilibrium conditions (low current, or small changes in the potential)[57]. Furthermore, a simple method to check if the capacitive current has a significant impact on the measured currents at faster rates is to do the following: Assume that $z$ amount of charge was measured during a fast discharge. If then the amount of charge from a slow recharge gives the same value, $z$, it is safe to assume that the current during the fast discharge was more or less 100% Faradaic[51].

## 2.4 Gibbs free energy and cell voltage

The cell voltage is another defining feature of the chemical reactions taking place inside the battery. The equilibrium (open-circuit) cell voltage ($V_{OC}$) is directly related to the changes in the free energy by[19]:

$$\Delta G = -nFV_{OC} \qquad \textit{(Eq. 2-10)}$$

where, $G$ is the Gibbs free energy (J/mol), $n$ is the number of electrons, F is the Faradays constant (F = 96485 C/mol).

Furthermore, the open-circuit voltage is given by the difference between the chemical potential of lithium in the anode ($\mu A$) and in the cathode ($\mu C$)[10, 19]:

$$V_{OC} = \frac{(\mu A - \mu C)}{F} \qquad \textit{(Eq. 2-11)}$$

For a battery with lithium metal as the anode, we normally assume that the chemical potential of the lithium metal is constant[58]. Thus, the obtained voltage curve from the battery reflects mainly the changes in the chemical potential of lithium inside the cathode material itself. Furthermore, the chemical potential of lithium in an intercalation compound is equal to the derivative of the free energy of the material with respect to Li concentration according to[59]:

$$\mu_{Li} = \frac{\delta g}{\delta x} \qquad \textit{(Eq. 2-12)}$$

where, g is the Gibbs free energy per $Li_xMA$ formula unit, where MA represents host chemistry (e.g. $FePO_4$ with M being the transition metal and A the anion unit), and $x$ denotes the fraction of available interstitial sites occupied by Li.

The direct connection between the Gibbs free energy and the measured voltage means that the occurrence of phase transformations due to variations in Li concentration will have clear signatures in the voltage profile[59]. How the chemical potential of lithium in the cathode affects the obtained voltage is shown in *Figure 2-3*.

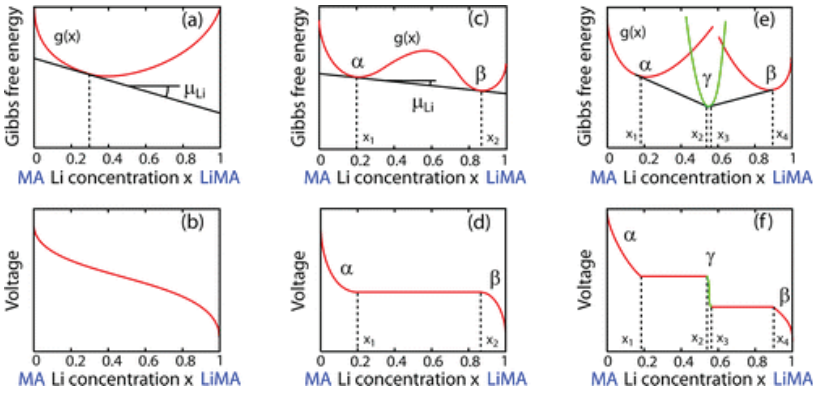


**Figure 2-3.** *Voltage curves are linearly related to the slope of the free energy of the electrode material. See the text for a description of the various cases*[59].

Solid-solution behaviour (a-$FePO_4$):

*Figure 2-3 a)* shows the electrode host material forming a solid solution with Li, as occurs in amorphous $FePO_4$, giving rise to a smooth sloping voltage curve as illustrated in *Figure 2-3 b)*. This is due to the chemical potential of lithium varying as a function of the amount of lithium intercalated. From a thermodynamic point of view the voltage of an intercalation electrode showing a solid-solution reaction is given by[60]:

$$E = E^0 + \frac{RT}{nF} ln\left(\frac{X}{1-X}\right) \qquad \textit{(Eq. 2-13)}$$

where, $X$ is the fraction of occupied intercalation sites, $E^0$ standard potential (V), R the universal gas constant (J/mol·K), $T$ the temperature (K), $n$ the number of electrons transferred (mol e/mol), and F is the Faraday's constant (C/mol e).

Another way to explain this behaviour can be done by utilizing Gibbs' phase rule, which states that the relation among the number of degrees of freedom ($f$) and the number of independent components ($c$), in a closed system at equilibrium is given by

$$f = c - p + n \qquad \textit{(Eq. 2-14)}$$

where, $n$ is the number of the intensive variables necessary to describe the system (except the mole fractions of the components in each phase), $p$ is the number of phases and $c$ the number of components[61]. In electrochemical studies, the intensive quantities are only temperature and pressure, which both are kept constant, so that $n = 0$. Here, we deal with a binary system ($c = 2$) and if only one phase exists in the electrode ($p = 1$), which gives $f = 1$. Meaning that the potential is a degree of freedom and therefore varies with the Li concentration [61-62].

Two-phase behaviour ($LiFePO_4$):

If the Li insertion is accompanied by a first-order phase transformation from a Li-poor phase to a Li-rich phase, as occurs in crystalline olivine $LiFePO_4$, the free energy curve will exhibit two local minima (assuming the host maintains the same crystal structure)[59], as illustrated in *Figure 2-3 c)*. As long as both phases co-exists the change in Gibbs free energy will be constant, resulting in a voltage curve that is independent on the Li concentration as illustrated in *Figure 2-3 d)*.

Again Gibbs' phase rule can also be used to explain this behaviour. If we use the values given for the solid-solution reaction above, but in this case the electrode contains two co-existing phases ($p = 2$), which results in $f = 0$. This means that no intensive variable (e.g. potential) can change [22, 61]. This behaviour is further illustrated in *Figure 2-4*.

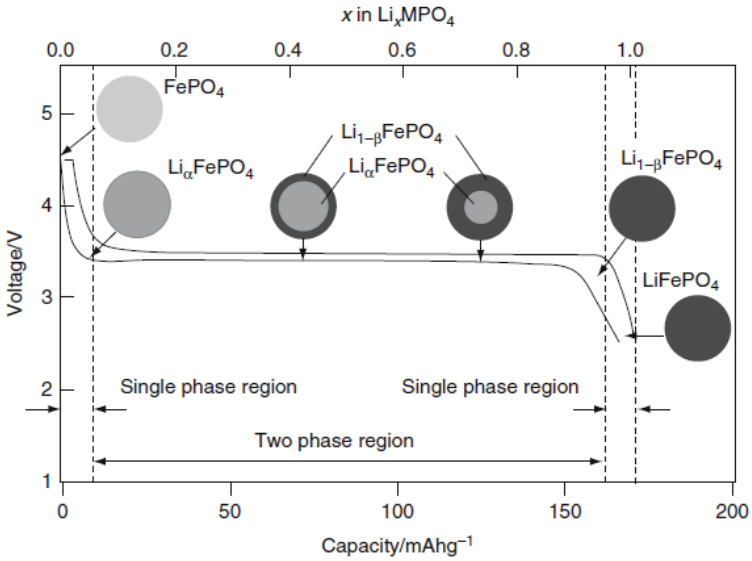


**Figure 2-4.** *Galvanostatic charge/discharge curves for crystalline $LiFePO_4$, showing two-phase behaviour*[63].

Several phase transitions ($V_2O_5$):

If the Li insertion is accompanied by more than one phase transition occurring over the whole composition range, as is the case for $V_2O_5$, the free energy curve will exhibit several local minima as illustrated in *Figure 2-3e)*. This results in steps in the voltage curve as illustrated in *Figure 2-3f)*, where

again the plateaus corresponds to a composition range where two phases co-exist in the electrode.

## 2.5 Electrochemical methods

There are several electrochemical methods which can be used to investigate the electrochemical properties of battery electrode materials [54, 57]. Normally, it is the cell voltage and the current that are the two main parameters of interest for many of these methods, where one often is controlled and the other is monitored. The previous mentioned Faraday's law in *Eq. 2-2* gives us the following relationship between the current (*i)* and the normalized reaction rate *v* (mol/s $m^2$) per electrode area A:

$$\frac{dQ}{dt} = i = nF\frac{dx}{dt} = nFAv \qquad \textit{(Eq. 2-15)}$$

This shows that the current flowing in the external circuit is proportional to the instantaneous rate of the redox reactions occurring inside the battery. Thus, the combined information we get from the voltage and the current can give information on both the kinetic and thermodynamic aspects of the electrode materials and the redox reactions occurring inside the battery[54]. In this work, two electrochemical techniques were used for investigation of the electrochemical properties of the deposited thin films, galvanostatic (GS) and cyclic voltammetry (CV).

## 2.5.1 Galvanostatic measurements

During a galvanostatic measurement a constant current is forced into or out of the battery, while the voltage is recorded as a function of time, see *Figure 2-5*.

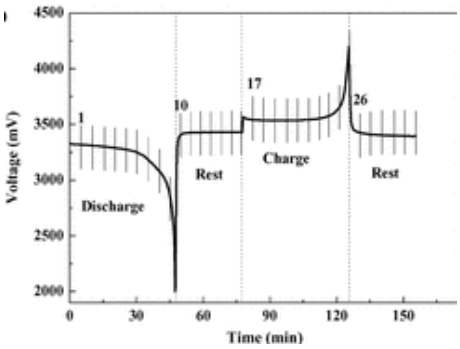


**Figure 2-5.** *Raw data collected from a galvanostatic measurement performed on $LiFePO_4$ at 1 C rate, in the potential window 2.0 – 4.2 V* [64].

The current used during a GS measurement is often given as a C-rate (mA/g). Therefore, before the measurement can be performed, the amount of active material has to be determined in order to calculate how large a current is needed for a chosen C-rate. Presenting the raw data from a GS measurement (voltage as a function of time) is not very practical, instead, the obtained data is often displayed as specific capacity, or the *x* amount of Li intercalated, as a function of the cell voltage, see *Figure 2-6*.

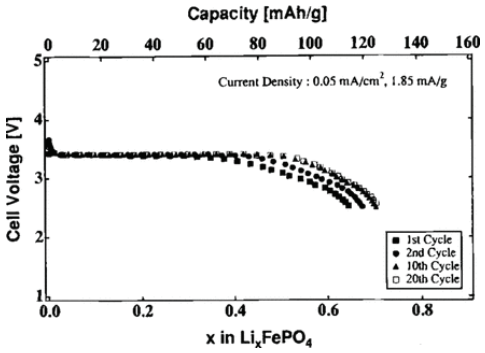


**Figure 2-6.** *Discharge curves of $LiFePO_4$ at 1.85 mA/g (~C/90).*[38]

## 2.5.2 Cyclic voltammetry

Cyclic voltammetry (CV) is one of the most versatile and useful techniques for investigation of the redox properties of a given material. CV is often the first experiment performed in an electrochemical study of a compound. The effectiveness of CV results from its capability to rapidly obtain information on the redox properties of a given material over a wide potential range. In addition, CV can provide information on both the thermodynamic properties and some of the kinetic aspects of the redox reaction. During a measurement the electrode potential (on the electrode of interest, the working electrode) is swept from an initial value ($E_i$) to a final value ($E_\lambda$) (versus a counter/reference electrode) at a constant scan rate $v$ (V/s). If time is given by $t$, the potential sweep is represented by:

$$E = E_i - vt \qquad \textit{(Eq. 2-16)}$$

Once the value $E_\lambda$ is reached the direction of the scan is reversed, maintaining the same scan rate $v$, until the potential reaches a second

endpoint value $E_{\lambda,2}$. A cyclic voltammogram is obtained by measuring the current running between the working and the counter electrode during the potential scan. The current can be considered as the response signal to the potential changes. The obtained current-potential curves can be represented as shown in *Figure 2-7*. The potential varies linearly with time, and it can sometimes be useful to think of the *x*-axis as a time axis. Furthermore, as *Figure 2-7 a)* shows, the conventional (by IUPAC) way is to display oxidation (charging) of the electrode as positive current (current going into the battery), and for reduction (discharging) of the electrode the current is negative (current going out of the battery). In cyclic voltammetry, the oxidation and reduction reactions are also referred to as anodic and cathodic processes, respectively. The basic parameters for a cyclic voltammogram, as shown in *Figure 2-7b)*, are explained in *Table 2-1* below.

| Parameter | Description |
|---|---|
| $E_{pf}$ | Potential of the forward peak |
| $E_{pr}$ | Potential of the return peak |
| $E_{\lambda}$ | Potential value at the inversion of the scan direction |
| $E_{\lambda,2}$ | $E_{\lambda,2}$ = potential value of the second endpoint |
| $i_{pf}$ | Current of the forward peak with respect to its baseline |
| $i_{pr}$ | Current of the return peak with respect to its baseline |
| $\Delta E_p$ | Peak-to-peak separation |
| $(i_{pr})_0$ | Current of the return peak with respect to the zero current baseline |
| $(i_f)_0$ | Current at the inversion potential with respect to the zero current baseline |

**Table 2-1.** *The basic parameters for a cyclic voltammogram.*[54]

Of these, the most important parameters are the anodic and cathodic peak currents and their respective potentials[65]. It is also worth noting that the area under the curve corresponds to the amount of charge stored (anodic part) or released (cathodic part) by the redox reactions.

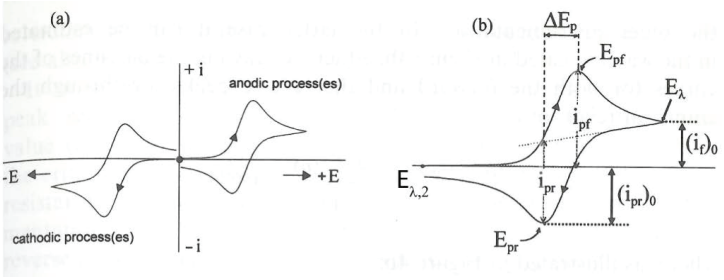


**Figure 2-7.** ***a)*** *The conventional signs of current and potentials in cyclic voltammetry.* ***b)*** *Basic parameters for a cyclic voltammogram: see the text for explanations* [54].

The behavior of the current during the potential scan can be understood by examining the concentration profile shown in *Figure 2-8c)*. If we consider an anodic scan, where Li-ions are extracted from the electrode, it is the Li-ions closest to the electrode surface that is extracted first. This creates a concentration gradient of Li-ions inside the electrode. During the scan the current will increase until all the lithium ions close to the surface are extracted. The current will then reach a maximum as the rate of reaction becomes limited by diffusion of Li-ions inside the electrode[52]. Furthermore, as Li-ions are continuously extracted from the electrode the Li concentration gradient inside the electrode becomes smaller and smaller. Since the flux of a diffusing specie is dependent on the concentration gradient along the direction of propagation, as given by Fick's first law[54] (see *Eq. 2-17*), the measured current starts to decrease as a result of the

ever-diminishing concentration gradient and the following decrease in flux of Li-ions.

$$-J_{Li}(x,t) = D_{Li}\,\frac{\delta c_{Li}(x,t)}{\delta x} \qquad \textit{(Eq. 2-17)}$$

where, $J$ is the flux of Li-ions, $D$ is the Li-ion diffusion coefficient in the electrode. This diffusion-limited behavior is the reason why the current-potential profile in a cyclic voltammogram goes through a maximum, before it starts to decrease.

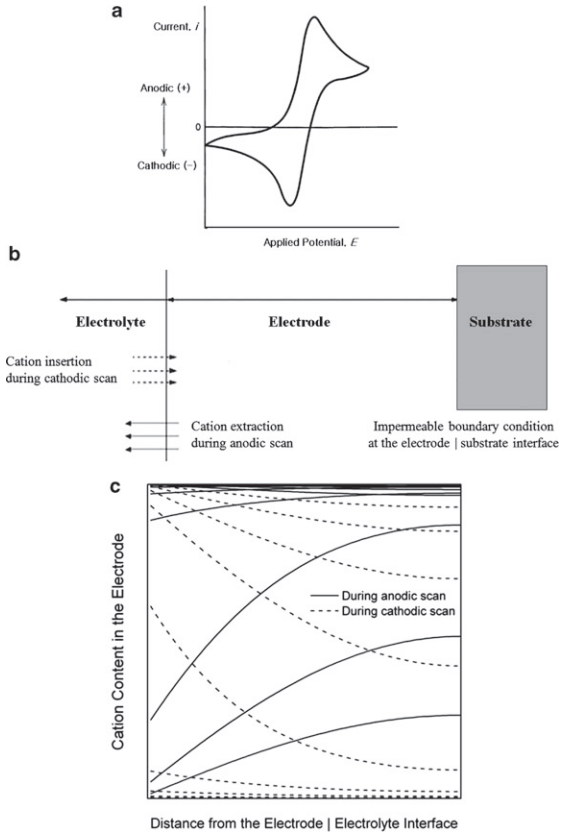


**Figure 2-8** ***a)*** *Typical shape of cyclic voltammogram,* ***b)*** *the cation (Li) movement during potential scan, and* ***c)*** *the expected potential (or time) dependence of the cation (Li) content profile* [66].

In cyclic voltammetry, a redox process is categorized as one of three main groups, depending on how it behaves during a measurement. It can be termed electrochemically reversible, quasireversible or irreversible. These terms have nothing to do with the chemical reversibility of a reaction, as a reversible redox reaction can show electrochemically irreversible behavior. The electrochemical reversibility of a reaction closely depends upon the rate of charge-transfer being sufficiently high to maintain the surface concentrations close to those demanded by the electrode potential through the Nernst equation. If the rate of mass transport is the limiting step, the process is termed electrochemical reversible (fast), and depending on how slow the charge-transfer reaction is, the reaction can be termed either quasireversible or irreversible. This also means that if the sweep rate is increased, a reversible reaction may transform into an irreversible one, if the rate of charge-transfer can be considered slow in comparison to the sweep rate.

The main points for these three categories can quickly be summarized as, (see also *Figure 2-9*):

- Electrochemical reversible processes have a small peak-to-peak separation that is independent on the sweep rate.

- A quasireversible process behaves reversible at low sweep rates, and irreversible at higher sweep rates.

- Electrochemical irreversible processes have a larger peak-to-peak separation that also increases with increasing sweep rate.

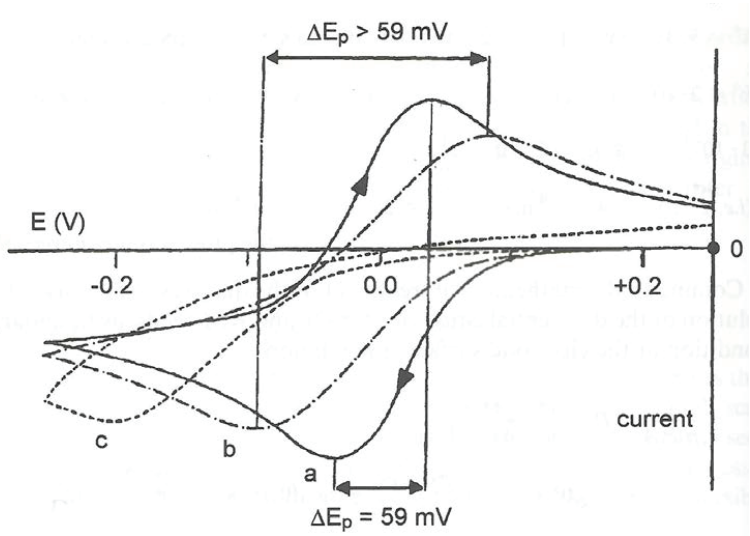


**Figure 2-9.** *Qualitative behavior of the cyclic voltammetric profiles for a redox process having features of: A) reversibility; b) quasireversibility; c) irreversibility. α = 0.5, $E^{0'}$ = 0V, T = 25°C.*[54]

The redox behavior of lithium intercalation electrodes are often termed as quasi- and irreversible processes in the literature, since the peak-to-peak separation often increases with increasing scan rate[67], even though they are also considered to be rate-limited by mass transport. Either way, all the terminology that was developed for describing the different processes that occur at an inert electrode in a solution containing redox active species, might not be completely consistent when applied to intercalation electrodes.

## 2.5.3 The effects of the sweep rate

The sweep rate can be varied from "slow-scans" $v \leq 0.1$ mV/s and upwards to faster scans. At low sweep rates we assume that the system is

close to equilibrium during the measurement, while at faster sweep rates kinetics start to influence the measured properties. As mentioned earlier, at faster sweep rates the electrical double layer contributes with a capacitance effect at the electrode-electrolyte interface. However, at small values of voltage sweep rate, typically $v \leq 1$ mV/s the capacity effects are small and can be ignored[57]. Therefore, low sweep rates are used for investigating the specific capacity and the thermodynamic properties of a given material, while measurements with increasing sweep rates can be used to investigate some of the kinetic aspects. The current flowing at one of the peaks during a CV-measurement is being limited by some mechanism, and as mentioned earlier, this limiting-mechanism for a $Li^+$ de/intercalation reaction is often considered to be the lithium solid-state diffusion in the electrode. Consequently, investigation of how the peak-currents change with increasing sweep rates, can give some information about the rate-limiting steps during the charge-storage mechanism. Here, a brief explanation for how this can be done will be given.

For a given redox reaction:

$$Ox + ne^- \leftrightarrow Red \qquad \textit{(Eq. 2-18)}$$

complex differential equations can be obtained by combining *Eq. 2-1* with Fick's laws of diffusion and some appropriate form of the Nernst equation[57]. From these equations an expression can be derived (through Laplace's transformations) that gives the maximum current (i.e. the current at the potential corresponding to the maximum of the peak) for a planar electrode during a CV-scan[54]:

$$i_p = 0.4463 \times A \times C_{Ox}^{*} \times \frac{n^3 \times F^3 \times D_{Ox} \times v}{\sqrt{R \times T}} \qquad \textit{(Eq. 2-19)}$$

which, at 25°C, gives what is called the Randles-Sevcik equation:

$$i_p = 2.69 \times 10^5 \times n^{3/2} \times A \times D_{Ox}^{1/2} \times C_{Ox}^{*} \times v^{1/2} \qquad \textit{(Eq. 2-20)}$$

Where:

$i_p$ = forward peak-current (A)

$n$ = number of electrons exchanged per molecule of $O_x$

$A$ = area of the electrode ($m^2$)

$D_{ox}$ = diffusion coefficient of Ox ($m^2/s$)

$C^*_{ox}$ = concentration of Ox (mol/l)

$v$ = potential scan rate (V/s)

This equation can be used to obtain information about many different properties of the redox couple / electrode material in question by analysing the relationship between the sweep rate and the peak current. However, in this work this equation has not been used to obtain any detailed information about parameters (i.e. the diffusion coefficient). Instead, it has been used to provide information on how a diffusion-controlled process correlates the sweep rate to the peak-current, which results in the following: If the electrode reaction in question is limited by diffusion, the peak-current ($i_p$) should scale with the square root of the sweep rate, $v^{1/2}$. Thus by plotting log $i_p$ vs. log $v$ a straight line should be obtained with a slope equal to 0.5 if the process is limited by diffusion. Diffusion limited behaviour is normally observed for most lithium battery intercalation electrodes[67-68], even in thin films and nanoparticles the $Li^+$ de/intercalation reactions show solid-state diffusion limited behaviour[7, 69].

However, the Randles-Sevcik equation (*Eq. 2-20*) is only valid for an electrochemical reversible system, and as mentioned earlier intercalation electrodes are often considered as electrochemically quasireverisble or irreversible processes. Nevertheless, the assumption of the peak current being proportional to the square root of the sweep rate is still valid, as the peak current for an irreversible system at 25°C is given as[54]:

$$i_p = 2.99 \times 10^5 \times n \times (\alpha \times n_\alpha)^{1/2} \times A \times D_{Ox}^{1/2} \times C_{Ox}^{*} \times v^{1/2} \qquad \textit{(Eq. 2-21)}$$

where, $n_\alpha$ is the number of electrons exchanged in the slowest step, α is a transfer coefficient (which often is equal to 0.5), the other parameters are the same as in the reversible case. Thus, regardless whether a given redox reaction is considered as an electrochemical reversible, quasireversible or irreversible process, the peak current obtained from a CV-measurement can be expected to be proportional to the square root of the scan rate (if the process is limited by diffusion).

Finally, as touched upon earlier, the dependence of the peak-to-peak separation ($E_p$) on the sweep rate can be used to identify if the rate constant for the charge-transfer reaction is fast or slow, i.e. if the process is reversible or irreversible. An example on how the peak-to-peak separation can be affected by the sweep rate is given in *Figure 2-10*. And as *Figure 2-10* illustrates, any electrochemical reversible process can be made to behave irreversible if only the sweep rate in a CV-measurement is increased high enough.

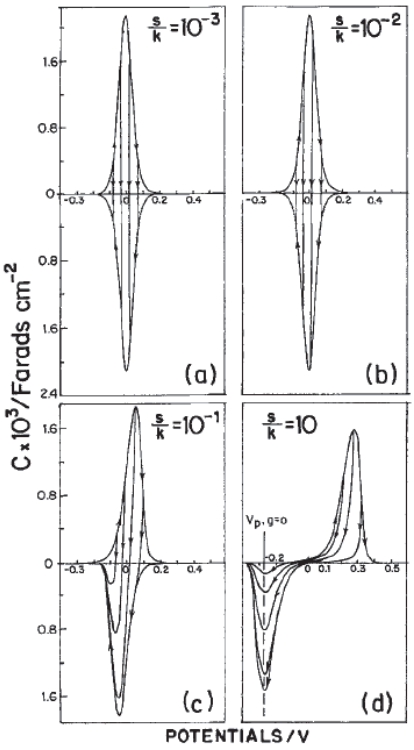


**Figure 2-10.** *Transition of cyclic voltammograms for pseudocapacitance of a single-state surface process from conditions of kinetic reversibility to irreversibility as the sweep rate, s, (V/s) is increased. The rate constant of the process is given by k.*[16b]

However, since the current increases as $v$ is increased, a larger sweep rate will shift $E_p$, due to uncompensated resistance. It moves systematically in a negative direction with increasing $v$ (for a reduction). Thus uncompensated resistance can have the insidious effect of mimicking the response found with heterogeneous kinetics limitations[55], which means that peak-to-peak

separations observed at high sweep rates are not necessarily due to kinetic limitations of the charge-transfer reaction.

### 2.5.4 Detailed analysis of diffusion and capacitive effects

Determination of the rate limiting step of an electrochemical reaction can be obtained through describing the maximum peak current with respect to the sweep rate by a power-law [67, 69b, 70]:

$$I_p = av^b \qquad \textit{(Eq. 2-22)}$$

where, $I_p$ is the peak current in A, $v$ is the sweep rate in V/s, $a$ and $b$ are adjustable coefficients. The b-exponent takes values between 0.5 and 1, whether the redox process is limited by diffusion of the active species (b = 0.5) according to *Eq. 2-20* and *Eq. 2-21*, or surface-controlled and thus behave in a capacitive manner (b = 1), according to *Eq. 2-9*.

By plotting a log $I_p$ vs. log $v$, the slope will be equal to 1 if the charge storage mechanism behaves in a capacitive manner, and equal to 0.5 if it instead is limited by diffusion. However, as the obtained *b*-values can change over the investigated sweep rate range, this basic representation does not accurately highlight the changes in the kinetic behaviour of the charge storage mechanism. A more detailed representation can be obtained by assuming that the total measured current can be divided into two contributions[71]. One part is considered to change with the sweep rate, while the other part changes with the square root of the sweep rate:

$$I_p = k_1 v + k_2 v^{1/2} \qquad \textit{(Eq. 2-23)}$$

,which can be rearranged as:

$$\frac{I_p}{v^{1/2}} = k_1 v^{1/2} + k_2 \qquad \textit{(Eq. 2-24)}$$

Two different contributions to the total measured current are thus observed. The current that originates from a charge storage mechanism that is not limited by solid-state diffusion is defined by the $k_1$ coefficient. A contribution to the total measured current that originates from diffusion-limited faradaic reactions is defined by the $k_2$ coefficient. Consequently, it becomes possible to determine the nature of the charge storage mechanism by calculating the ratio $k_1/k_2$, and one can also easily observe the changes in the reaction kinetics as a function of the sweep rate.

By plotting *Eq.2-24*, $k_1$ would be the slope of the curve, and $k_2$ its *y*-intercept. If there are any significant changes to the kinetics of the charge storage mechanism as the sweep rate is varied, this will be revealed in the plot as two or more straight lines, each with their own unique slope and *y*-intercept.

## 2.5.5 Coulombic efficiency

The coulombic efficiency describes the efficiency with which electrons are transferred into a system facilitating an electrochemical reaction. The charge necessary to charge a cell ($Q_{charge}$) is always higher than the charge released during discharge ($Q_{discharge}$). This is caused by an incomplete conversion of the charging current into utilizable reaction products. However, lithium batteries have close to 100% coulombic efficiency[10] and it is given as:

$$\eta_C = \frac{Q_{discharge}}{Q_{charge}} \qquad \textit{(Eq. 2-25)}$$

## 2.6 Kinetic effects on the rate performance

The kinetic effects discussed so far in this chapter are more or less responsible for why the amount of energy we can obtain from a battery decreases as the current rate increases. The equilibrium voltage of a cell will be reduced when current is drawn due to kinetic limitations. This process is known as overvoltage or polarization (η), and how these different effects influence the voltage of a cell can be summarized as[18]:

$$E = E^0 - [(\eta_{ct})_a + (\eta_{ct})_c] - [(\eta_c)_a + (\eta_c)_c] - iR_i = iR$$

Where:

$E^0$ is the equilibrium voltage of the cell.

$(\eta_{ct})_a$, $(\eta_{ct})_c$ is the charge-transfer overpotential at the anode and cathode, respectively.

$(\eta_c)_a$, $(\eta_c)_c$ is the concentration polarization (diffusion gradients) at the anode and the cathode, respectively.

$i$ = operating current of cell.

$R_i$ = internal resistance of the cell.

R = apparent cell resistance.

The influence of these different effects on the voltage is also shown in *Figure 2-11*.

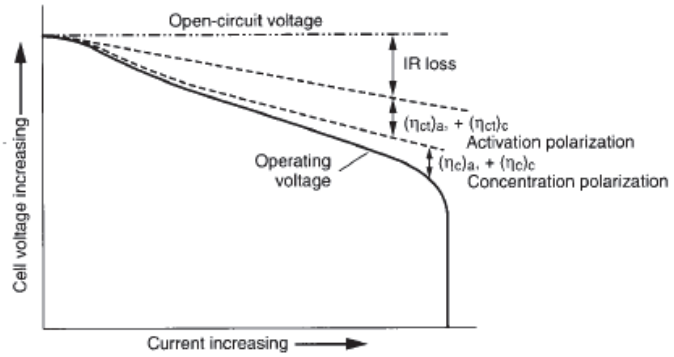


**Figure 2-11.** *The influence of different kinetic effects on the cell potential, as a function of operating current.*[57]

The charge-transfer overpotential is caused by the fact that the speed of the charge-transfer through the electrode/electrolyte phase-boundary is limited. This overpotential is related to the operating current through the Butler-Volmer equation, as mentioned earlier in this chapter.

Concentration polarization arises from limited mass transport capabilities within a system. This can be manifest as inadequate diffusion to and from an electrode surface of the active species that are required to sustain a reaction, as mentioned earlier in the cyclic voltammetry chapter. The influence of this effect on the voltage is more complex, however, simply put it affects the cell voltage through the Nernst equation[10].

The internal resistance arises from the combined resistance of the electrolyte, the materials used in construction of the cell, and the current-collector.

The energy lost due to the resulting voltage drops from all of these different effects is converted to waste heat (which can present a safety hazard if large currents are used). However, when the rates are increased, less capacity (charge) will also be accessible from the electrode material itself. This loss of capacity is not converted to waste heat, and (in the case of a discharge) the amount of unused lithium ions remains instead in the electrode. This is due to mass-transport limitations (diffusion), where a given amount of the lithium ions simply do not have enough time to be extracted from the electrode before the cut-off voltage is reached and the discharge terminated, leading to an incomplete discharge. The same kinetic limitations apply for a fast charge as well, however, in this case the battery will only be partially charged even though it stopped at its cut-off voltage.

As a final note regarding voltage drops: Thin film electrodes, due to low currents, provide some advantages as the data distortion from the internal resistance is less for them, than for batteries with higher amounts of active masses[72]. This therefore makes thin film electrodes ideal model systems for investigation of material and size dependent electrochemical properties.

# 3 The Atomic Layer Deposition Technique

The atomic layer deposition technique has a central role in this work, being the main synthesis method. In this chapter, a general introduction to the ALD technique will be given, before highlighting the prior art regarding deposition of battery cathodes with ALD. Finally, some comments will be given on deposition of lithium containing materials with ALD, as this topic deserves some special attention.

## 3.1 Description of the technique

Atomic layer deposition relies on successive, separated and self-limiting gas-solid phase reactions, between volatile precursors and active sites on the surface. *Figure 3-1* shows one ALD cycle of deposition of aluminum oxide ($Al_2O_3$) from the precursor pair, trimethylaluminum (TMA) and water. As illustrated in *Figure 3-1*, when the first precursor (TMA) is introduced into the reaction chamber, it binds to the substrate surface through a chemisorption reaction. When the surface is saturated, no more reactions can take place (the precursor does not react with itself). The excess precursor is then purged with an inert gas ($N_2$), leaving one monolayer of TMA chemisorbed to the surface. Once the second precursor (water) is introduced into the reaction chamber, it will react with the previously chemisorbed monolayer of TMA, forming aluminum oxide. Again, no more reactions can take place once all the chemisorbed TMA have reacted. The reaction chamber is then purged with an inert gas ($N_2$), ending the cycle and (ideally) one monolayer of $Al_2O_3$ has been deposited. The cycle is repeated

as many times as needed in order to achieve the desired film thickness. Several extensive and good review articles on this topic have been written which will provide more depth and insight into ALD [73].

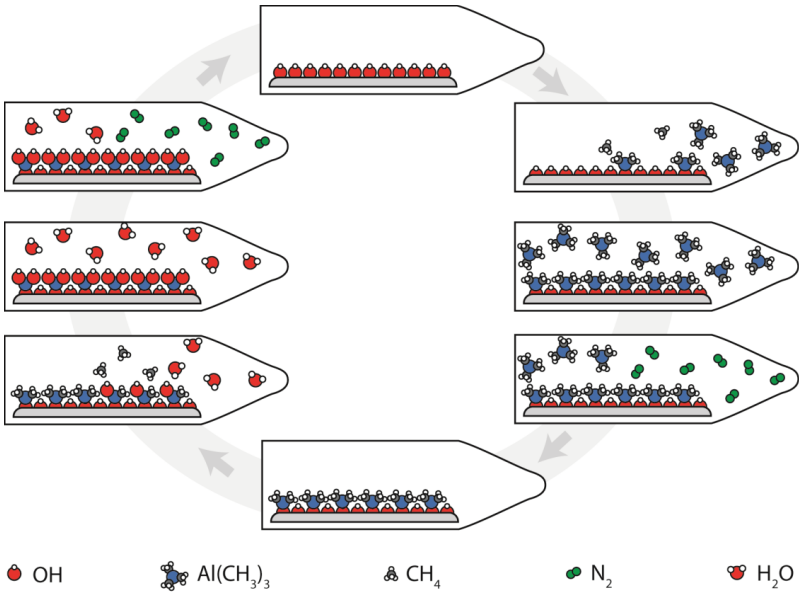


**Figure 3-1.** *Illustration of an ALD cycle for deposition of $Al_2O_3$[74].*

## 3.2 Why use ALD for batteries?

This question has been touched upon earlier in the previous chapters, where one of the benefits mentioned was having a thin film electrode with precisely controlled and conformal thickness. However, one solution to meet the increasing power requirements following the rapid advances in integrated microsystems, is 3D structuring of batteries, leading to increased mass of active material and enhanced kinetics. Furthermore, a transition from liquid to solid electrolytes would also greatly increase the safety, enable a more complex design, and allow for utilization of higher voltage chemistries. Since one of the main strengths of the ALD technique is that it can provide conformal and pinhole free films on complex substrates, makes it one of the most promising techniques for realization of 3D nano-structured batteries [6b].

## 3.3 ALD of lithium battery cathode materials

The lithium battery cathode materials that have previously been deposited by ALD, are mainly unlithiated transition metal oxides such as $TiO_2$[75], $MnO_2$[76], $Co_3O_4$[77], $(Co,Fe)_3O_4$[78], $V_2O_5$[79] and NiO[80].

The lithiated cathode materials reported so far are $LiCoO_2$[81], $LiFePO_4$[82], and $LiMn_2O_4$[83].

### 3.3.1 $FePO_4$ and $LiFePO_4$

Deposition of $FePO_4$ and $LiFePO_4$ by ALD is for the first time presented in this work in *Papers I* [37b] and *II*, respectively. Some of the findings in *Paper II* was presented in 2010[82]. Although, as *Paper II* shows, $Li_xFePO_4$ is a more precise way to describe the "$LiFePO_4$" films obtained in this work. These depositions were carried out by combining the deposition process of iron oxide from $Fe(thd)_3 + O_3$, with the phosphate process from $Me_3PO_4 + H_2O + O_3$. The $Li(thd) + O_3$ process was added for incorporation of lithium.

The number of phosphate materials deposited by ALD is still relatively limited and an overview is given in *Table 3-1*.

| Material | Phosphate precursor | Year | Refs. |
|---|---|---|---|
| $AlPO_4$ | $Me_3PO_4 + H_2O$ | 1995 | [84] |
| $AlPO_4$ | $P_2O_5 + H_2O$ | 1998 | [85] |
| $Ca_xP_yO_z$ | $Me_3PO_4 + O_3$ | 2009 | [86] |
| $LaPO_4$ | $Me_3PO_4 + (H_2O + O_3)$ | 2010 | [87] |
| $LiFePO_4$ | $Me_3PO_4 + (H_2O + O_3)$ | 2010 | [82] |
| $Ti_x(PO_4)_y$, $Al_x(PO_4)_y$ | $Me_3PO_4$ | 2012 | [88] |
| $Ti_x(PO_4)_y$ | $Me_3PO_4 + H_2O$ | 2012 | [89] |
| $Li_3PO_4$ | $Me_3PO_4$ | 2012 | [90] |

**Table 3-1.** *An overview of phosphate deposition processes with ALD.*

*Table 3-2* gives an overview of a selection of iron containing oxides that previously have been demonstrated grown by ALD, using a number of different iron sources. For a more complete overview, the review by Miikkulainen *et al.* is recommended [73a].

| Material | Iron precursor | Year | Refs. |
|---|---|---|---|
| $Fe_2O_3$ | $Fe(acac)_3 + O_2$ | 2002 | [91] |
| $Fe_2O_3$ | $Fe(thd)_3 + O_3$ | 2005 | [92] |
| $Fe_2O_3$ | $Fe_2(O^tBu)_6 + H_2O$ | 2007 | [93] |
| $Fe_2O_3$ | $FeCp_2 + O_2$ | 2008 | [94] |
| $(Fe, Co)_3O_4$ | $Fe(thd)_3 + O_3$ | 2008 | [78] |

**Table 3-2.** *An overview of iron containing oxides deposited by ALD.*

$Fe(thd)_3$ was chosen as the iron precursor in this work as our group have a considerable amount of experience with this precursor[92]. Similarly, $Me_3PO_4$ was selected as the phosphate precursor based on experience we acquired from an prior investigation of deposition of $LaPO_4$ with ALD[87], which used $La(thd)_3$ together with $Me_3PO_4$. In addition, both $Fe(thd)_3$ and $Me_3PO_4$ are easy to handle and relatively stable towards air exposure.

### 3.3.2 $V_2O_5$

The first deposition of a cathode material for lithium batteries by ALD was reported in 2003 by deposition of $V_2O_5$[79a]. *Table 3-3* gives an overview over a selection of reported $V_2O_5$ depositions. Again, for a more complete overview of work done on deposition of vanadium oxides in general, the review by Miikkulainen *et al.* is recommended [73a].

| Material | Iron precursor | Year | Refs. |
|---|---|---|---|
| $V_2O_5$ (amorphous) | $VO(O^iPr)_3 + H_2O$ | 2003 | [79a] |
| $V_2O_5$ (crystalline) | $VO(O^iPr)_3 + O_3$ | 2013 | [95] |
| $V_2O_5$ (crystalline) | $VO(thd)_2 + O_3$ | 2013 | [50] |

**Table 3-3.** *An overview of vanadium pentoxide deposition processes with ALD.*

The ALD process used for deposition of the $V_2O_5$ films investigated in *Paper IV* in this work is described in Ref. [50]. Samples obtained from this ALD process were chosen for electrochemical investigation in this work mainly based on two reasons: The first reason was that it is a new ALD process, and there exist no prior reports on the electrochemical properties of films based on this process. The second reason was, as mentioned earlier, that this process also gives films with highly textured surfaces consisting of crystalline nano-sheets of $V_2O_5$. As a highly textured surface combined with short lithium diffusion distances was expected to enhance the electrochemical performance, it was therefore extra interesting to see how the electrochemical properties of these films would compare to what is previously reported for $V_2O_5$.

### 3.3.3 ALD of lithium containing materials

Deposition of lithium containing films by ALD was first reported in 2009, where Li(thd) was combined with $O_3$ to from $Li_2CO_3$[96]. As only a few years have passed since the ALD community was introduced to Li-based ALD processes, this field is still quite immature. Today 11 different reported types of Li-precursors exists and an overview of these is given in *Paper V* [97]. However, there apparently are additional challenges with respect to Li-based ALD processes than normally encountered. There is still no universal robust Li-precursor which can be combined with most other systems. The combined experience in our group has shown surprisingly many incompatibilities between processes, which still may seem arbitrary. Furthermore, in some deposition processes the normal surface-limited ALD behaviour does not seem to be fulfilled, yet a homogeneous material may be obtained [83]. The lack of surface limited reactions may be due to that lithium is mobile during deposition leading to a more bulk controlled

mechanism. In addition, some of the Li-containing materials obtained during deposition can act as a water reservoir. The different challenges encountered when developing lithium based ALD processes are also an topic of discussion in *Paper V* [97].

# 4 Experimental Methods

In this work, several standard characterization techniques have been used to investigate both the as-deposited and heat treated thin films deposited by ALD. A quick introduction to all of these techniques will be given in this chapter, together with the respective instruments. As the electrochemical methods used in this work was previously explained in detail in the theory chapter, only instrument details will be mentioned here.

## 4.1 Structural Characterization

### 4.1.1 X-ray diffraction (XRD)

Two different instruments were used in order to characterize the crystallinity of the as-deposited and heat treated films: A Bruker D8 Discover diffractometer equipped with a Ge(111) monochromator providing Cu-K$\alpha_1$ radiation and using a LynxEye detector, and a Siemens D5000 diffractometer equipped with a Göbel mirror providing parallel Cu-K$\alpha$ radiation. The measurements were carried out in conventional $\theta$-$2\theta$ reflection mode with sample rotation. Only crystallographic planes that are parallel to the substrate will be detected during this type of measurement. Resulting in that not all reflections will necessarily be observed for a thin film, as film growth dynamics may sometimes lead to oriented growth.

### 4.1.2 Grazing incidence X-ray diffraction (GI-XRD)

Grazing incidence X-ray diffraction (GI-XRD) utilizes a small incident angle of the X-ray beam in order to increase both the illuminated area and the optical path through the thin film material. As a result, signals from the substrate are greatly suppressed, making this technique very suitable for structural characterization of thin films. Furthermore, as this technique is not limited to only detecting crystallographic planes that are parallel to the substrate, it makes a great addition to the θ-2θ reflection mode. The instrument used in this work was a Siemens D5000 equipped with a Göbel mirror providing parallel Cu-Kα radiation, with an incident angle of $\omega = 0.5^{o}$.

### 4.1.3 X-ray reflectivity (XRR)

X-ray reflectivity (XRR) is based on reflectivity of X-rays at low incident angles. During a measurement, the intensity of the reflected X-rays is measured as a function of the incident angle. Periodical intensity oscillations will appear when the incident angle becomes larger than a specific material dependent value, called the critical angle. These oscillations originate from interference between the X-rays reflected from the surface of the film and from the interface between the film and the substrate. The periodicity of these oscillations are related to the thickness of the film, the overall decrease in intensity as a function of the incident angle is related to the surface roughness, and the critical angle is determined by the film density. Two instruments were utilized for XRR in this work: A Siemens D5000 equipped with a Göbel mirror providing parallel Cu-Kα radiation, and a Bruker AXS D8 Discover diffractometer equipped with a Göbel mirror providing parallel

Cu-K$\alpha_1$ radiation with a LynxEye detector, where the obtained data was fitted using the GenX software.

### 4.1.4 X-ray fluorescence (XRF)

In X-ray fluorescence (XRF), atoms in the sample of interest are exited by X-rays and as they relax back to their ground state (or a lower orbital), X-rays are emitted. The energy of the emitted X-rays is characteristic for each element and its intensity is dependent on the amount of a given element in the sample. Quantative information can be extracted, such as the ratio between different elements in the sample, as well as the total amount of deposited mass. Furthermore, this method can normally not detect elements that are lighter than Ne. In this work X-ray fluorescence spectroscopy was performed using a Philips PW2400 and the obtained data was analysed with the UniQuant software.

### 4.1.5 Atomic force microscopy (AFM)

In atomic force microscopy (AFM), a small tip (~10 – 35 nm radius) is scanned across an area of the sample surface in a *xy*-pattern. In this manner, information about the surface roughness and topography, in addition to crystallite sizes and shapes can be obtained. In this work AFM was conducted in tapping mode using a Park Systems XE-70 together with the XEI-software package.

### 4.1.6 Scanning electron microscopy (SEM)

In scanning electron microscopy (SEM), an electron beam is scanned across an area of the sample surface in a *xy*-pattern. Through detection of the resulting back-scattered and secondary electrons a topographical and compositional picture of the sample surface can be constructed. In this work SEM was done using a FEG-SEM FEI Nova NanoSEM 650.

### 4.1.7 Spectroscopic ellipsometry (SE)

Spectroscopic ellipsometry (SE) is an optical analysis technique for investigating the thickness and the optical properties (e.g. refractive indexes) of thin films. In this work the SE measurements were done using a J.A. Woollam alpha-SE spectroscopic ellipsometer together with the CompleteEase software package. The obtained data were fitted to a Cauchy function based on their optical transparency.

### 4.1.8 Time-of-flight elastic recoil detection analysis (TOF-ERDA)

The time-of-flight elastic recoil detection analysis (TOF-ERDA) performed in this work was done by bombarding the target sample with an 8 MeV 79Br or 12 MeV 63Cu ion-beam from a pelletron accelerator. Atoms from the target recoils out of the sample, as the incoming ion-beam interacts and scatters with them. Both the energy and velocity of the recoiled atoms is measured simultaneously, from which elemental depth profiles can be obtained. With TOF-ERDA all the atoms of the samples, including lithium, can be quantitatively depth profiled. Thus, it is one of the few techniques capable to determine the concentration of lithium in a sample.

## 4.2 Electrochemical Investigation

### 4.2.1 Coin-Cell Assembly

The electrochemical properties of the thin film electrodes were investigated in CR2032 coin cells. Cell assembly was carried out inside an MBraun Labmaster glovebox filled with argon atmosphere, with water and oxygen levels below 0.1 ppm. Metallic lithium was used as anode, and the as-deposited thin films on 15.8 mm-diameter 316 stainless steel disks were used as cathodes. The liquid electrolyte consisted of 1M $LiClO_4$ in 1:1 mixture of ethyl carbonate (EC)/dimethyl carbonate (DMC). A Whatman glass microfiber sheet was used as the separator membrane.

### 4.2.2 Electrochemical measurements

Both cyclic voltammetry and galvanostatic measurements were performed at room temperature with a Bio-Logic MPG-2 multichannel battery cycler.

# 5 Results and Discussion

The current thesis has cumulated in five papers or manuscripts explaining the development of electroactive cathode materials using ALD. The core focus has been on development and characterisation of electroactive iron phosphates (*Papers I-III*). The thesis is the first in our research group where electrochemical characterisation has been in significant focus. These tools were also applied for characterisation of the electrochemical properties of highly textured vanadium oxide films made by ALD (*Paper IV*). An overview of lithium based processes is finally given in *Paper V*.

An introduction of the papers and their findings is given here in a natural chronological order of development, although the practical order of conduction was different. Some comments on this are given during discussions of paper II.

## 5.1 Paper I - High-performing iron phosphate for enhanced lithium ion solid state batteries as grown by atomic layer deposition

*Paper I* present the development of the ALD process for deposition of $FePO_4$ from the precursors $Fe(thd)_3 + O_3$ and $Me_3PO_4 + (H_2O + O_3)$. The electrochemical properties of a 46 nm thick film as lithium battery cathode were also reported. The electrochemical properties of this film revealed two particularly interesting features. The electrode showed the highest reported specific capacity for an amorphous $FePO_4$ electrode at current rates of 1 C,

see *Figure 5-1*. In addition, the capacity increased during cycling, which is not normally observed for lithium intercalation electrodes. These observations lead us to believe that amorphous $FePO_4$ might possess some excellent, but hidden, electrochemical properties. Amorphous $FePO_4$ has not been extensively investigated in the literature, and where it has been reported, the electrochemical properties are usually rather poor. Therefore, one could imagine that the true electrochemical properties of this material could have been concealed by other effects, such as the thickness of the electrodes/particles used in the prior investigations. Further investigation of how electrode thickness influenced the electrochemical properties of this material was carried out in *Paper III*.

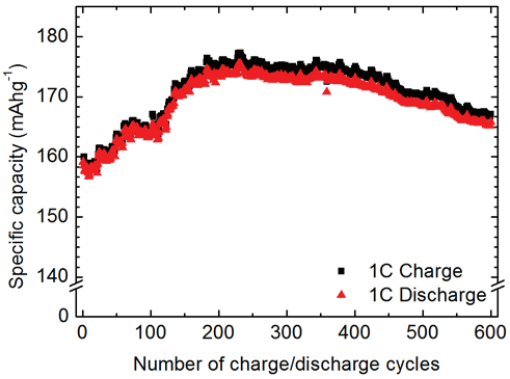


***Figure 5-1.*** *Cycling performance of the amorphous $FePO_4$ thin films between 2.0 – 4.0 V at 1 C rate.*

## 5.2 Paper II - Deposition of lithium containing iron phosphate by atomic layer deposition

*Paper II* presents the efforts to incorporate lithium into the $FePO_4$ process reported in *Paper I*, in order to obtain the well-known cathode material, olivine-type $LiFePO_4$. The lithium process chosen for this was Li(thd) + $O_3$, as this was one of the two first lithium processes that was introduced to the ALD community in 2009. The second process of Li($O^tBu$) + $H_2O$ was also preliminary tested together with the $FePO_4$ process, however, this resulted in uncontrolled growth and large amounts of $Li_3PO_4$ was deposited. The fact that this attempt resulted primarily in $Li_3PO_4$ is retrospectively not so strange when one realize that an ALD process for deposition of $Li_3PO_4$ by combining Li($O^tBu$) directly with $Me_3PO_4$ was later reported by Hämäläinen *et al.* in 2012[90].

Chronologically, the work with *Paper II* was the first task that was conducted, inspired by successful deposition of both $LaPO_4$ and $AlPO_4$, and several lithium based processes in our group. The work with the Li(thd) + $O_3$ process began well, and we rather quickly managed to obtain crystalline $LiFePO_4$ through heat treatment of the deposited films in reducing atmosphere, see *Figure 5-2*. The $LiFePO_4$ phase was identified by X-ray diffraction, and these findings were presented at the Baltic ALD conference in 2010. However, soon after we had presented the results we began to realize that there were apparent problems with this process. The situation was further complicated by the fact that we lacked a good method for measuring the amount of lithium incorporated into the films. We initially choose to control the lithium content by varying the amounts of lithium pulses added to the $FePO_4$ process, before heat treating the films and characterise for the $LiFePO_4$ phase, as proof of incorporation of lithium.

However, we quickly realised that heat treatment of identical samples did not necessarily result in crystallization of the $LiFePO_4$ phase. Based on our prior success, we assumed that something was wrong with the equipment, in particular the ALD reactor.

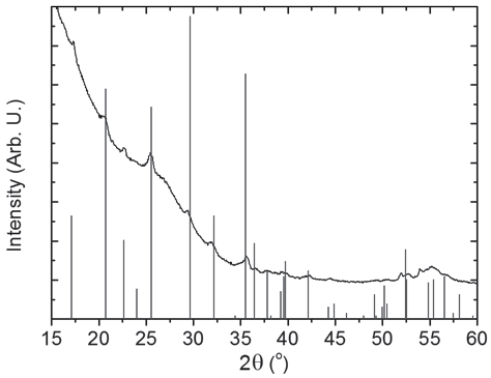


**Figure 5-2.** XRD d*iffractogram measured by GI-XRD of a 50 nm $LiFePO_4$ film, heat treated for 20 hours at 500 ºC in reducing atmosphere. The vertical lines represents olivine-type $LiFePO_4$ PDF 40-1499.*

Thus, two years with many different approaches quickly passed by while we tried to reproduce the first successful results. During these two years, we managed to reproduce the $LiFePO_4$ sample three times, and every time we believed we had finally solved the problem. During this period, we had begun to use the TOF-ERDA technique to determine the Li-content, which confirmed our growing suspicion that it was the ALD process itself which was problematic, and not the equipment. Samples obtained from the same substrate during a deposition run, showed different and varying lithium contents. Furthermore, the samples where only the $LiFePO_4$ phase could be observed by X-ray diffraction, showed a lithium content corresponding to $Li_{0.5}FePO_4$, only half of the lithium that we anticipated, see Figure *5-3*.

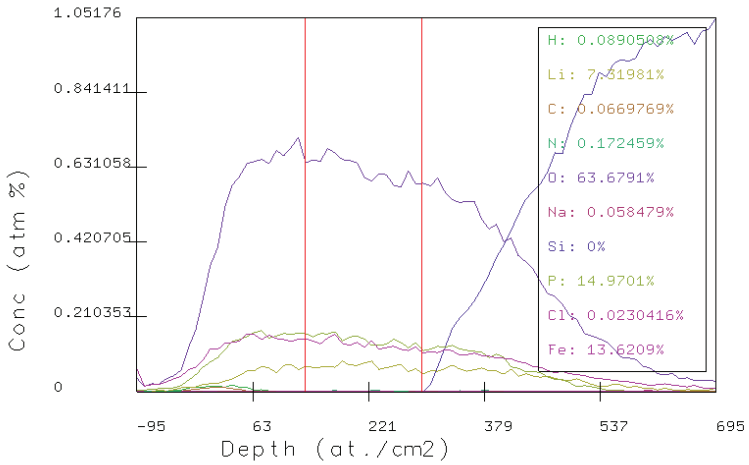


**Figure 5-3.** *TOF-ERDA depth-profile on a heat treated sample where the $LiFePO_4$ phase had been identified by GI-XRD.*

Later, we discovered that some Li-based ALD processes seem to display a more bulk-controlled mechanism, rather than the surface-controlled mechanism which one normally relates to ALD-processes. This is discussed in more detail in *Paper V*, however, if the $LiFePO_4$ deposition process is governed by a bulk-controlled mechanism it would help explain the varying amounts of lithium incorporated into the films, resulting in a less reproducible process. If we have used too short lithium pulsing times for achieving a saturated bulk growth, the amount of lithium incorporated into the films is then more dependent on the actual amount of precursor molecules delivered to the reaction chamber. It would be like using too short pulsing times in a normal ALD process, resulting in thickness gradients and a less reproducible process. However, for the lithium process the thickness gradients could instead be manifested as varying lithium content inside the bulk of the deposited film.

## 5.3 Paper III - Surprising Rapid Intercalation Pseudocapacitance Effects in Amorphous $LiFePO_4$

As already mentioned, *Paper III* was a continuation of the preliminary electrochemical investigation of the amorphous $FePO_4$ electrodes presented in *Paper I*. In this paper we investigated the thickness dependent electrochemical properties of electrodes with thicknesses ranging from 12 to 93 nm. The first finding in this paper revealed that the film thicknesses, on the nm-level, play a crucial role regarding the electrochemical performances of these electrodes. We observed that any added mass, for films thicker than ~50 nm, does not seem to be electrochemically active. This finding highlights the importance of uniform films with precise control of the thickness for optimization of the electrochemical performance of this material. This probably also applies for other materials exhibiting poor electronic or ionic conductivity.

However, the main findings in this paper was quite unexpected, as it turns out that the amorphous $FePO_4$ electrodes exhibit rather exotic properties, which, to our knowledge, have only been reported once before for a lithium intercalation electrode. This effect is termed rapid intercalation pseudocapacitance, and means that lithium ions can be inserted and extracted from the electrodes without being rate-limited by solid-state diffusion. The consequence of this is that the electrode can operate under extreme conditions (charged and discharged in seconds) without suffering from too large kinetic losses, which affects the specific capacity and the voltage. Surprisingly, the kinetics of these amorphous electrodes shows that they are comparable to those found in supercapacitors, which only utilize surface processes for the charge storage mechanism. In fact, as *Figure 5-4*

shows, these amorphous electrodes exhibit both the lifetime behaviour and rate-performance comparable to that of supercapacitors, where the initial capacity for a 23 nm electrode is only reduced by 24% after 10 000 cycles at 320 C.

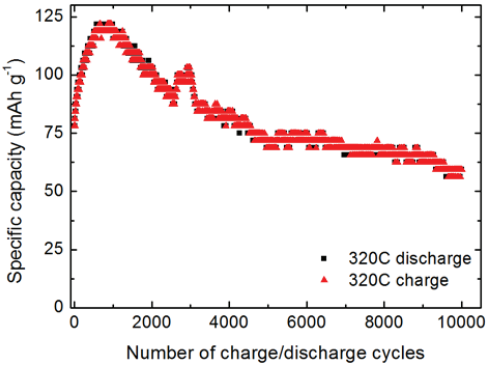


**Figure 5-4.** *Cycling performance of a 23 nm thick amorphous $FePO_4$ electrode cycled between 2.0 – 4.0 V at 320 C.*

Furthermore, the kinetics of the lithium intercalation/deintercalation reactions in these amorphous electrodes seems to undergo a self-enhancing effect. As *Figure 5-4* illustrates, the capacity increases significantly during the first 700 cycles at 320 C. *Figure 5-5* shows in more detail how the charge storage kinetics of the 23 nm thick electrode is affected by the 700 galvanostatic cycles at 320 C. The △-symbols illustrate the behaviour of the electrode before the galvanostatic cycling, while the ▽-symbols illustrate the behaviour after the treatment. The coloured area represents the amount of charge storage originating form a diffusion-limited mechanism. What can be seen is that after the 700 cycles at 320 C, the capacity of the 23 nm electrode is significantly less affected by the sweep rate, indicating faster kinetics. In addition, the electrode shows significantly less influence from diffusion-limited processes on the charge storage mechanism. In fact, after

the galvanostatic cycling the 23 nm electrode shows kinetics comparable to that of the 12 nm thick electrode. This clearly shows that the repeated insertion and extraction of lithium ions during the galvanostatic cycling has somehow resulted in faster transport of lithium ions in the electrode, suggesting that the material has undergone structural rearrangements resulting in more optimized lithium transport pathways. Despite such arrangements, the electrode remains X-ray amorphous.

Finally, for the 12 nm electrode a specific capacity of 90 mAh/g could be reversibly accessed at 2560 C, corresponding to a specific power above 1 MW/kg $FePO_4$. This is one order of magnitude higher than the highest reported specific power for the crystalline olivine-type $LiFePO_4$, and three orders of magnitude higher than typical specific powers obtained from lithium batteries.

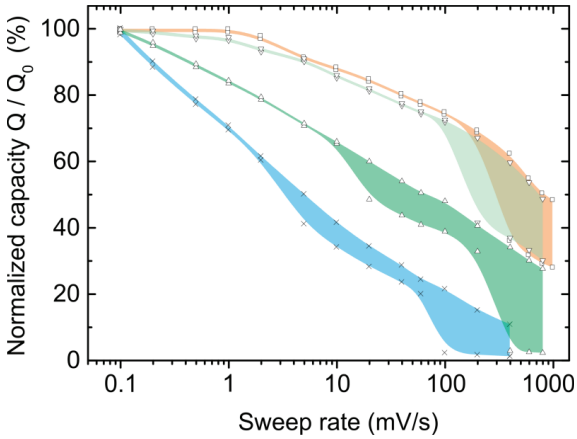


**Figure 5-5.** *Normalized capacity of amorphous $FePO_4$ electrodes with the following thicknesses: 46 nm (×), 23 nm (△,▽), 12 nm (□), illustrating the impact of diffusion-limited capacity on the total stored charge (colored area) as a function of sweep rate.*

# 5.4 Remarks on amorphous materials and facile kinetics

## 5.4.1 Amorphous materials, an overlooked group?

The electrochemical properties observed for the amorphous $FePO_4$ electrodes in *Paper I*, but mainly in *Paper III*, suggest that amorphous materials might possess some very interesting properties, which might have been overlooked by a research field mostly being dominated by crystalline materials. In fact, a very recent paper published in Science by Ceder *et al.*[98] questions the tradition that only crystalline cathodes are sought after.

Regarding the $FePO_4$ electrodes, if the flexibility of the amorphous structure is responsible for both the excellent lifetime, as well as the self-enhancing effect, one could argue that amorphous materials exhibit some superior properties when compared to crystalline materials. This should at least warrant more investigation.

Another possible benefit of amorphous materials was highlighted in Ref.[16a] where a specific capacity of 60 mAh $g^{-1}$ at 400 C and a specific power of 170 kW $kg^{-1}$ was obtained for 50 nm sized nanoparticles of crystalline $LiFePO_4$ coated with a thin amorphous layer. This behavior was limited to nanoparticles with an amorphous surface layer, suggesting that the coating was responsible for the ultra-high rate performance. They speculated whether the amorphous layer enhances the charge-transfer kinetics of the surface by providing lithium sites with a wide range of energies that can be more easily matched to the electrolyte.

## 5.4.2 Where do batteries end and supercapacitors begin?

Another interesting discussion which surfaces for the thinnest electrodes reported in this work is that if the observed electrochemical behaviour is similar to that of supercapacitors in every aspect, are they then no longer batteries? If so, where do batteries end and supercapacitors begin?

A very recent perspective with that exact topic was published in Science by Dunn *et al.*[68] . They make the claim that a nanostructured battery is still a battery as long as some key features remain in a certain way. The key-features they mention are:

*1)* The peak-to-peak separation in a CV measurement. This separation has to be small and independent on the sweep rate, in order to claim that the material under investigation is a supercapacitor and not a battery. However, if the material under investigation is a battery material which is engineered at the nanoscale so that a large fraction of $Li^+$ storage sites are on the surface or near surface region, they claim that the battery can behave in a pseudocapacitive way, provided the peak-to-peak separation is independent on the sweep rate.

*2)* The kinetic analysis of peak currents from CV, where for most battery materials, even as very thin films (< 10 nm), the peak currents scales with the square root of the sweep rate[67-68, 99] ($v^{1/2}$), indicating a diffusion-limited charge storage processes. For a capacitive process, as found in supercapacitors, the peak currents scales with the sweep rate ($v$).

They further state that if claims are to be made that battery materials behaves as a “high-energy density supercapacitor” they need to be evaluated

at the rates where supercapacitors devices are used (1 min discharge/charge, i.e. 60 C). They end by stating that the prospects of developing materials with the energy density of batteries and the power density and cycle life of supercapacitors is an exciting direction that has yet to be realized. Should this goal be approached by increasing the power density of battery materials or increasing the energy density of supercapacitors?

Based on the observed properties for the thinner electrodes of amorphous $FePO_4$ tested in this work one could argue that a material with the energy density of batteries and the power density and cycle life of supercapacitors have indeed been realized. We base our claim not only from testing the battery materials at the high-rates of 60 C as Dunn *et al.* suggests, but rather all the way up to 2560 C.

The thinner $FePO_4$ electrodes obtained in this work display pseudocapacitive properties in that the peak-to-peak separation is independent on the sweep rate up until a certain sweep rate. According to Dunn *et al.*, the only way for a battery material to show this behaviour is for the charge storage to occur solely at the surface or near-surface region. However, the amorphous $FePO_4$ electrodes do not only utilize charge storage at the surface or the near-surface region, yet they still do show this pseudocapacitive behaviour. A quick note regarding analysis of the peak-to-peak separation: We have to keep in mind that the true rate performance of the electrode can be concealed at higher sweep rates, due to the internal resistance in the battery contributing to the observed peak-to-peak separation.

Furthermore, the thinner $FePO_4$ electrodes show complete capacitive behaviour for lithium de/intercalation even at high sweep rates, a property

that has only been observed before in crystalline mesoporous $Nb_2O_5$[67] and then through the exotic effect termed "rapid intercalation pseudocapacitance". Thus, our claim is that the thinner amorphous $FePO_4$ electrodes obtained in this work can be regarded as batteries that behave like supercapacitors through the rapid intercalation pseudocapacitance effect.

## 5.5 Paper IV - High Power Nano-Structured $V_2O_5$ Thin Film Cathodes by Atomic Layer Deposition

In *Paper IV* we studied the thickness dependent electrochemical properties of $V_2O_5$ thin films, where the deposition process resulted in a rather unusual, for an ALD process, highly nano-structured surface of crystalline $V_2O_5$. During this investigation, we also observed an influence of the thickness on the electrochemical properties, however, not as dominating as observed for the amorphous $FePO_4$ electrodes. What we observed was that when these electrodes were cycled at low rates all electrodes, regardless of thickness, showed comparable specific capacities. Meaning that for all film thicknesses, a similar percent of the total cathode was electrochemically active during the slow rates. The influence of the film thickness became first apparent when the rates were increased. The thinnest sample deposited from 500 ALD cycles showed the best capacity retention at increasing C-rates, while the thickest sample deposited from 5000 ALD cycles showed the worst capacity retention at increasing C-rates. Since the sample deposited from 500 ALD cycles showed the best kinetics, its rate-capability and lifetime behaviour was tested further. For this electrode we found that ~20% of its 1 C-capacity could reversibly be accessed at 960 C, corresponding to a specific power of 395 kW/kg $V_2O_5$. Furthermore, cycling

performance at 120 C, see *Figure 5-6*, reveals that the specific capacity remains above 80% for 1500 cycles. This combination of both high specific power and excellent lifetime has, to our knowledge, not been reported before for $V_2O_5$.

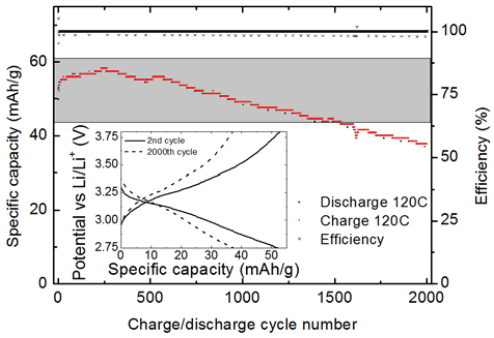


**Figure 5-6.** *Cycling stability at 120 C between 2.75 – 3.80 V. The grey band indicates a window with less than 80% capacity loss relative to the initial capacity (55 mAh/g at 120 C). Coulombic efficiency is close to 100%. Inset: charge and discharge curves shown for the 2nd and 2000th cycle.*

## 5.6 Paper V - Atomic layer deposition of functional films for Li-ion microbatteries

The combined efforts in our research group enabled us to compile a review over the lithium-based processes reported so far. This is a rapidly increasing field where several papers utilizing such processes have been reported since its submission, and a complete overview is difficult to obtain. We hope that this paper can function as a suitable entry point into this field, but we also realize that updates to this review are required in the near future.

# 6 Concluding Remarks

The aim of this work was to synthesize thin films of a few selected lithium battery cathode materials by ALD, and further investigate how the electrochemical performance of these materials was influenced by the film thickness at the nm-level. Here, we will first quickly present some of the main findings in each paper, before a more general conclusion will be made at the end.

An ALD process for deposition of $FePO_4$ was developed, utilizing the precursor pairs of $Fe(thd)_3 + O_3$ together with $Me_3PO_4 + (H_2O + O_3)$. This process yields amorphous films, and has an ALD window from 246 to 360 ºC. As-deposited amorphous 46 nm thick films shows excellent electrochemical behaviour, where theoretical capacities are reached at a current rate of 1 C. Furthermore, an increase in the capacity is observed during galvanostatic cycling at 1 C, resulting in a 3% increase from the initial capacity after 600 cycles.

Lithium was successfully incorporated into the $FePO_4$ process by addition of the $Li(thd) + O_3$ process at 246 ºC, yielding amorphous $Li_xFePO_4$ films. Heat treatment of the obtained films under reducing atmosphere resulted in crystallization of the olivine-type $LiFePO_4$ phase. However, TOF-ERDA measurements revealed that the process is rather unstable, and the highest lithium content obtained corresponds to an overall composition of $Li_{0.5}FePO_4$. In retrospect it might be a good thing that the ALD process for the more well-know battery cathode $LiFePO_4$ did not succeed, as then the

exiting electrochemical properties of the amorphous $FePO_4$ material might not have been discovered.

Electrochemical investigation of amorphous $FePO_4$ electrodes with thicknesses from 12 to 93 nm reveals a strong correlation between the electrode thickness and the electrochemical properties. Any added mass by increasing the thickness above 46 nm does not seem to be electrochemically active, resulting in greatly reduced electrochemical performance. However, record breaking electrochemical properties were, surprisingly, found for the thinner films with thicknesses of 12 and 23 nm. Analysis by cyclic voltammetry reveals that the peak currents scales with the sweep rate, demonstrating that these electrodes exhibit extremely facile kinetics, comparable to that found for supercapacitors. Specific powers above 1 MW/kg $FePO_4$ are observed for the 12 nm thick electrode, where ~50% of its theoretical capacity can still be reversibly accessed. The 23 nm electrode shows excellent lifetime behaviour, where the initial capacity is only reduced by 24% after 10 000 cycles at 320 C. In addition, self-enhancing kinetics are observed for the 23 nm electrodes suggesting some form of optimization of the lithium ion transport during cycling. This self-enhancing mechanism results in a 75 % increase in the capacity during galvanostatic cycling at the ultra high-rates of 320 C.

The thickness dependent electrochemical properties of highly nano-textured $V_2O_5$ were also investigated. The sample deposited from 500 ALD cycles showed superior rate-performance compared to the other tested electrode thicknesses ranging from 250 – 5000 ALD cycles. Specific powers of 395 kW/kg $V_2O_5$ could be obtained, comparable with that of a supercapacitor, where 20% of its 1 C capacity could be reversible accessed. In addition to displaying high power capabilities, the 500 ALD electrodes could also be

cycled for 1500 cycles at 120 C before the initial capacity dropped below 80%. Such a combination of high power capabilities and lifetime behaviour has, to our knowledge, not been reported before for $V_2O_5$.

Regarding lithium based ALD-processes, the main conclusion is, that lithium is a challenging element to work with both regarding characterization and process development. However, this is a rapidly increasing field and it is certain that in the years to come a lot of progress will be made, together with an increased fundamental understanding of lithium based ALD-processes.

Thus, through the initial goal to investigate the electrochemical properties of a few selected cathode materials, we have in this work shown the importance of conformal and precise thickness control for electrodes with poor electronic/ionic conductivities, for optimized performance in lithium batteries. Furthermore, we have also shown that through precise thickness control we can reveal the true rate capabilities of a material. This is achieved through a combination of factors such as, conformal and precisely controlled thickness of the electrode to the current collector. In addition, the electrodes contains no binders or conductive additives, which otherwise could had concealed the true rate capabilities of the electrode material itself.

From our investigations we can also report, for the first time, that the exotic phenomenon termed rapid intercalation pseudocapacitance is observed in an amorphous material. These amorphous $FePO_4$ electrodes show the highest reported specific power regardless of modification for the well-know battery material $LiFePO_4$, and to our knowledge, the highest reported value for any battery cathode material. These results show that amorphous materials,

which have been an overlooked group, might offer hope for substantial improvements in the performance of lithium batteries.

Finally, the possibilities that the ALD technique offers, being able do deposit thin high-rate materials together with the capabilities of utilizing high-surface area substrates, are promising for development of an energy device that combines the energy density of batteries with the power density of supercapacitors.

# 7 Future Perspectives

Today, the performances of lithium batteries are already being optimized towards their intended applications through selection of proper cathode and anode materials. Being able to further tailor the power-performance through nanostructured electrodes with precisely controlled thickness is an exciting development.

ALD is one of the promising candidates that can enable the required thickness control on high-surface area substrates. Deposition of lithium battery materials with ALD is still a relatively immature field, however, the field is expanding rapidly. There is a continuous development of new deposition processes for all battery components such as anodes, electrodes, and cathodes. The progress in this field has likely been slowed down by the many unexpected challenges connected with lithium based ALD-processes. However, as more and more lithium precursors are tested and an increasing understanding of the fundamental principles governing these processes is obtained, there is no doubt that there will be many substantial improvements in this field.

As already mentioned, ALD is a promising technique for manufacturing 3D nano-structured high-surface electrodes. By combining this aspect with the possibility of depositing electrode materials exhibiting pseudocapacitive behaviour, one opens for exciting structures which combines the energy density of batteries with the power density of supercapacitors.

Finally, it also appears that ALD has a bright future in production of 3D-structured all-solid-state batteries, again mostly due to the fact that these batteries require conformal and pinhole free films, on high-surface area substrates. One of the key-features for the electrode materials in all-solid-state batteries is that they do not undergo large volume expansion during intercalation of lithium. Mechanical stress in all-solid state batteries will undoubtedly reduce the lifetime behaviour of the battery stack. In this aspect, amorphous materials might have beneficial properties as they normally exhibit very small volume expansion during Li insertion/deinsertion[98]. A small volume expansion during insertion and extraction of lithium should also enhance the lifetime behaviour of the electrode. Of course, amorphous materials lack the stable voltage plateaus often found in crystalline materials, due to lack of phase transitions. This will limit the use of amorphous materials in applications that require a constant voltage. However, the lack of phase transition might also be one of the key features giving amorphous materials an extreme rate capability, as it is one of the suggested key-features for the occurrence of the exotic effect of rapid intercalation pseudocapacitance.

Battery research is an enormous and challenging field to work in. However, I believe that the findings in this work show that the ALD technique has a place in this rapidly developing and exiting field. In the years to come, I have no doubt that ALD will contribute to improvements for lithium batteries. Some of these improvements by ALD might come in the form of thin surface coatings on bulk-materials, thin electrodes on high surface-area substrates, or the realization of an all-solid-state 3D-structured battery.

# 8 References

[1] B. Scrosati and J. Garche, *Journal of Power Sources* **2010**, *195*, 2419-2430.

[2] a) M. Armand and J. M. Tarascon, *Nature* **2008**, *451*, 652-657; b) J. B. Goodenough and Y. Kim, *Chemistry of Materials* **2010**, *22*, 587-603.

[3] J. M. Tarascon and M. Armand, *Nature* **2001**, *414*, 359-367.

[4] K. Zaghib, A. Mauger and C. M. Julien, *Journal of Solid State Electrochemistry* **2012**, *16*, 835-845.

[5] R. Marom, S. F. Amalraj, N. Leifer, D. Jacob and D. Aurbach, *Journal of Materials Chemistry* **2011**, *21*, 9938-9954.

[6] a) C. Marichy, M. Bechelany and N. Pinna, *Advanced Materials* **2012**, *24*, 1017-1032; b) H. C. M. Knoops, M. E. Donders, M. C. M. van de Sanden, P. H. L. Notten and W. M. M. Kessels, *Journal of Vacuum Science & Technology A* **2012**, *30*; c) M. Knez, K. Niesch and L. Niinisto, *Advanced Materials* **2007**, *19*, 3425-3438.

[7] J. Come, P. L. Taberna, S. Hamelet, C. Masquelier and P. Simon, *Journal of the Electrochemical Society* **2011**, *158*, A1090-A1093.

[8] P. T. Keyser, *Journal of near Eastern Studies* **1993**, *52*, 81-98.

[9] B. Dibner, *Alessandro Volta and the electric battery*, F. Watts, **1964**, p.

[10] C. Daniel and J. O. Besenhard, *Handbook of battery materials*, John Wiley & Sons, **2011**, p.

[11] R. Moshtev and B. Johnson, *Journal of Power Sources* **2000**, *91*, 86-91.

[12] M. S. Whittingham, *Science* **1976**, *192*, 1126-1127.

[13] G. Pistoia, *Lithium batteries: new materials, developments, and perspectives*, Elsevier Science Ltd, **1994**, p.

[14] B. Scrosati, *Electrochimica Acta* **2000**, *45*, 2461-2466.

[15] a) P. H. L. Notten, F. Roozeboom, R. A. H. Niessen and L. Baggetto, *Advanced Materials* **2007**, *19*, 4564-4567; b) L. Baggetto, R. A. H. Niessen, F. Roozeboom and P. H. L. Notten, *Advanced Functional Materials* **2008**, *18*, 1057-1066.

[16] a) B. Kang and G. Ceder, *Nature* **2009**, *458*, 190-193; b) B. E. Conway, *Journal of the Electrochemical Society* **1991**, *138*, 1539-1548.

[17] Z. G. Yang, J. L. Zhang, M. C. W. Kintner-Meyer, X. C. Lu, D. W. Choi, J. P. Lemmon and J. Liu, *Chemical Reviews* **2011**, *111*, 3577-3613.

[18] M. Park, X. C. Zhang, M. D. Chung, G. B. Less and A. M. Sastry, *Journal of Power Sources* **2010**, *195*, 7904-7929.

[19] M. S. Whittingham, *Chemical Reviews* **2004**, *104*, 4271-4301.

[20] P. Simon and Y. Gogotsi, *Nature Materials* **2008**, *7*, 845-854.

[21] Y. J. Lee and A. M. Belcher, *Journal of Materials Chemistry* **2011**, *21*, 1033-1039.

[22] A. K. Padhi, K. S. Nanjundaswamy and J. B. Goodenough, *Journal of the Electrochemical Society* **1997**, *144*, 1188-1194.

[23] L. X. Yuan, Z. H. Wang, W. X. Zhang, X. L. Hu, J. T. Chen, Y. H. Huang and J. B. Goodenough, *Energy & Environmental Science* **2011**, *4*, 269-284.

[24] R. Malik, A. Abdellahi and G. Ceder, *Journal of the Electrochemical Society* **2013**, *160*, A3179-A3197.

[25] R. Amin, J. Maier, P. Balaya, D. P. Chen and C. T. Lin, *Solid State Ionics* **2008**, *179*, 1683-1687.

[26] C. B. Zhu, K. Weichert and J. Maier, *Advanced Functional Materials* **2011**, *21*, 1917-1921.

[27] R. Malik, D. Burch, M. Bazant and G. Ceder, *Nano Letters* **2010**, *10*, 4123-4127.

[28] H. Huang, S. C. Yin and L. F. Nazar, *Electrochemical and Solid State Letters* **2001**, *4*, A170-A172.

[29] S. Nishimura, G. Kobayashi, K. Ohoyama, R. Kanno, M. Yashima and A. Yamada, *Nature Materials* **2008**, *7*, 707-711.

[30] S. Y. Chung, J. T. Bloking and Y. M. Chiang, *Nature Materials* **2002**, *1*, 123-128.

[31] P. S. Herle, B. Ellis, N. Coombs and L. F. Nazar, *Nature Materials* **2004**, *3*, 147-152.

[32] N. Ravet, A. Abouimrane and M. Armand, *Nature Materials* **2003**, *2*, 702-702.

[33] C. A. J. Fisher, V. M. H. Prieto and M. S. Islam, *Chemistry of Materials* **2008**, *20*, 5907-5915.

[34] P. Gibot, M. Casas-Cabanas, L. Laffont, S. Levasseur, P. Carlach, S. Hamelet, J. M. Tarascon and C. Masquelier, *Nature Materials* **2008**, *7*, 741-747.

[35] T. K. Pietrzak, L. Wewior, J. E. Garbarczyk, M. Wasiucionek, I. Gorzkowska, J. L. Nowinski and S. Gierlotka, *Solid State Ionics* **2011**, *188*, 99-103.

[36] Y. S. Hong, K. S. Ryu, Y. J. Park, M. G. Kim, J. M. Lee and S. H. Chang, *Journal of Materials Chemistry* **2002**, *12*, 1870-1874.

[37] a) C. L. Li and Z. W. Fu, *Journal of the Electrochemical Society* **2007**, *154*, A784-A791; b) K. B. Gandrud, A. Pettersen, O. Nilsen and H. Fjellvag, *Journal of Materials Chemistry A* **2013**, *1*, 9054-9059.

[38] A. K. Padhi, K. S. Nanjundaswamy, C. Masquelier, S. Okada and J. B. Goodenough, *Journal of the Electrochemical Society* **1997**, *144*, 1609-1613.

[39] S. W. Kim, J. Ryu, C. B. Park and K. Kang, *Chemical Communications* **2010**, *46*, 7409-7411.

[40] Y. J. Lee, H. Yi, W. J. Kim, K. Kang, D. S. Yun, M. S. Strano, G. Ceder and A. M. Belcher, *Science* **2009**, *324*, 1051-1055.

[41] M. S. Whittingham, *Journal of the Electrochemical Society* **1976**, *123*, 315-320.

[42] D. M. Yu, S. T. Zhang, D. W. Liu, X. Y. Zhou, S. H. Xie, Q. F. Zhang, Y. Y. Liu and G. Z. Cao, *Journal of Materials Chemistry* **2010**, *20*, 10841-10846.

[43] V. Shklover, T. Haibach, F. Ried, R. Nesper and P. Novak, *Journal of Solid State Chemistry* **1996**, *123*, 317-323.

[44] R. Baddour-Hadjean, V. Golabkan, J. P. Pereira-Ramos, A. Mantoux and D. Lincot, *Journal of Raman Spectroscopy* **2002**, *33*, 631-638.

[45] N. A. Chernova, M. Roppolo, A. C. Dillon and M. S. Whittingham, *Journal of Materials Chemistry* **2009**, *19*, 2526-2552.

[46] G. Sudant, E. Baudrin, B. Dunn and J. M. Tarascon, *Journal of the Electrochemical Society* **2004**, *151*, A666-A671.

[47] C. Delmas, H. Cognacauradou, J. M. Cocciantelli, M. Menetrier and J. P. Doumerc, *Solid State Ionics* **1994**, *69*, 257-264.

[48] R. Baddour-Hadjean, J. P. Pereira-Ramos, C. Navone and M. Smirnov, *Chemistry of Materials* **2008**, *20*, 1916-1923.

[49] K. Takahashi, S. J. Limmer, Y. Wang and G. Z. Cao, *Journal of Physical Chemistry B* **2004**, *108*, 9795-9800.

[50] E. Ostreng, O. Nilsen and H. Fjellvag, *Journal of Physical Chemistry C* **2012**, *116*, 19444-19450.

[51] C. J. Patrissi and C. R. Martin, *Journal of the Electrochemical Society* **1999**, *146*, 3176-3180.

[52] S. W. Kim, S. B. Lee and S. I. Pyun, *Solid State Electrochemistry I: Fundamentals, Materials and their Applications* **2011**, 133-177.

[53] A. S. Arico, P. Bruce, B. Scrosati, J. M. Tarascon and W. Van Schalkwijk, *Nature Materials* **2005**, *4*, 366-377.

[54] P. Zanello, *Inorganic electrochemistry: theory, practice and applications*, Royal Society of Chemistry, **2003**, p.

[55] A. J. Bard and L. R. Faulkner, **2001**.

[56] D. Y. Qu and H. Shi, *Journal of Power Sources* **1998**, *74*, 99-107.

[57] D. Linden and T. Reddy in *Handbook of Batteries, 2002*, *Vol.* McGraw-Hill.

[58] N. Meethong, H. Y. S. Huang, S. A. Speakman, W. C. Carter and Y. M. Chiang, *Advanced Functional Materials* **2007**, *17*, 1115-1123.

[59] A. Van der Ven, J. Bhattacharya and A. A. Belak, *Accounts of Chemical Research* **2013**, *46*, 1216-1225.

[60] B. E. Conway, V. Birss and J. Wojtowicz, *Journal of Power Sources* **1997**, *66*, 1-14.

[61] K. E. Aifantis, S. A. Hackney and R. V. Kumar, *High energy density lithium batteries: materials, engineering, applications*, John Wiley & Sons, **2010**, p.

[62] C. V. Ramana, A. Mauger, F. Gendron, C. M. Julien and K. Zaghib, *Journal of Power Sources* **2009**, *187*, 555-564.

[63] R. J. Brodd in *Batteries for Sustainability*, *Vol.* Springer, **2012**.

[64] H. H. Chang, C. C. Chang, H. C. Wu, M. H. Yang, H. S. Sheu and N. L. Wu, *Electrochemistry Communications* **2008**, *10*, 335-339.

[65] P. T. Kissinger and W. R. Heineman, *Journal of Chemical Education* **1983**, *60*, 702-706.

[66] S.-I. Pyun, H.-C. Shin, J.-W. Lee and J.-Y. Go, *Electrochemistry of Insertion Materials for Hydrogen and Lithium*, Springer, **2012**, p.

[67] V. Augustyn, J. Come, M. A. Lowe, J. W. Kim, P. L. Taberna, S. H. Tolbert, H. D. Abruna, P. Simon and B. Dunn, *Nature Materials* **2013**, *12*, 518-522.

[68] P. Simon, Y. Gogotsi and B. Dunn, *Science* **2014**, *343*, 1210-1211.

[69] a) T. Brezesinski, J. Wang, J. Polleux, B. Dunn and S. H. Tolbert, *Journal of the American Chemical Society* **2009**, *131*, 1802-1809; b) H.

Lindstrom, S. Sodergren, A. Solbrand, H. Rensmo, J. Hjelm, A. Hagfeldt and S. E. Lindquist, *Journal of Physical Chemistry B* **1997**, *101*, 7717-7722.

[70] T. Brezesinski, J. Wang, S. H. Tolbert and B. Dunn, *Nature Materials* **2010**, *9*, 146-151.

[71] J. Wang, J. Polleux, J. Lim and B. Dunn, *Journal of Physical Chemistry C* **2007**, *111*, 14925-14931.

[72] D. Pletcher, *Microelectrodes : Theory and Applications* **1991**, *197*, 3-16.

[73] a) V. Miikkulainen, M. Leskela, M. Ritala and R. L. Puurunen, *Journal of Applied Physics* **2013**, *113*; b) M. Leskela and M. Ritala, *Thin Solid Films* **2002**, *409*, 138-146; c) M. Leskela and M. Ritala, *Angewandte Chemie-International Edition* **2003**, *42*, 5548-5554.

[74] I. Vee in *Fluorholdige hybridmaterialer med atomlagsavsetting: Syntese og karakterisering*, *Vol.* (Ed. i. Universitetet i Oslo Fysisk), Oslo, **2012**, p. book.

[75] a) A. Turkovic, A. Drasner, D. Sokcevic, M. Ritala, T. Asikainen and M. Leskela, *Journal De Physique Iv* **1995**, *5*, 1133-1139; b) W. Wang, M. Tian, A. Abdulagatov, S. M. George, Y. C. Lee and R. G. Yang, *Nano Letters* **2012**, *12*, 655-660.

[76] a) O. Nilsen, S. Foss, A. Kjekshus and H. Fjellvag, *Journal of Nanoscience and Nanotechnology* **2008**, *8*, 1003-1011; b) O. Nilsen, H. Fjellvag and A. Kjekshus, *Thin Solid Films* **2003**, *444*, 44-51.

[77] K. B. Klepper, O. Nilsen and H. Fjellvag, *Thin Solid Films* **2007**, *515*, 7772-7781.

[78] M. Lie, K. B. Klepper, O. Nilsen, H. Fjellvag and A. Kjekshus, *Dalton Transactions* **2008**, 253-259.

[79] a) F. Lantelme, A. Mantoux, H. Groult and D. Lincot, *Journal of the Electrochemical Society* **2003**, *150*, A1202-A1208; b) K. Le Van, H. Groult,

A. Mantoux, L. Perrigaud, F. Lantelme, R. Lindstrom, R. Badour-Hadjean, S. Zanna and D. Lincot, *Journal of Power Sources* **2006**, *160*, 592-601.

[80] E. Lindahl, M. Ottosson and J. O. Carlsson, *Chemical Vapor Deposition* **2009**, *15*, 186-191.

[81] M. E. Donders, H. C. M. Knoops, W. M. M. Kessels and P. H. L. Notten, *Atomic Layer Deposition Applications 7* **2011**, *41*, 321-330.

[82] K. Gandrud, A. Pettersen, O. Nilsen and H. Fjellvåg, *Hamburg, Germany* **2010**, 16-17.

[83] V. Miikkulainen, A. Ruud, E. Ostreng, O. Nilsen, M. Laitinen, T. Sajavaara and H. Fjellvag, *Journal of Physical Chemistry C* **2014**, *118*, 1258-1268.

[84] M. Nieminen, L. Niinisto and R. Lappalainen, *Mikrochimica Acta* **1995**, *119*, 13-22.

[85] M. Tiitta, E. Nykanen, P. Soininen, L. Niinisto, M. Leskela and R. Lappalainen, *Materials Research Bulletin* **1998**, *33*, 1315-1323.

[86] M. Putkonen, T. Sajavaara, P. Rahkila, L. T. Xu, S. L. Cheng, L. Niinisto and H. J. Whitlow, *Thin Solid Films* **2009**, *517*, 5819-5824.

[87] H. Sønsteby, E. Østreng, O. Nilsen and H. Fjellvåg, *Baltic ALD 2010, Conference Proceedings* **2010**.

[88] J. Hamalainen, J. Holopainen, F. Munnik, M. Heikkila, M. Ritala and M. Leskela, *Journal of Physical Chemistry C* **2012**, *116*, 5920-5925.

[89] M. K. Wiedmann, D. H. K. Jackson, Y. J. Pagan-Torres, E. Cho, J. A. Dumesic and T. F. Kuech, *Journal of Vacuum Science & Technology A* **2012**, *30*.

[90] J. Hamalainen, J. Holopainen, F. Munnik, T. Hatanpaa, M. Heikkila, M. Ritala and M. Leskela, *Journal of the Electrochemical Society* **2012**, *159*, A259-A263.

[91] M. de Ridder, P. C. van de Ven, R. G. van Welzenis, H. H. Brongersma, S. Helfensteyn, C. Creemers, P. Van Der Voort, M. Baltes, M.

Mathieu and E. F. Vansant, *Journal of Physical Chemistry B* **2002**, *106*, 13146-13153.

[92] M. Lie, H. Fjellvag and A. Kjekshus, *Thin Solid Films* **2005**, *488*, 74-81.

[93] J. Bachmann, J. Jing, M. Knez, S. Barth, H. Shen, S. Mathur, U. Gosele and K. Nielsch, *Journal of the American Chemical Society* **2007**, *129*, 9554-+.

[94] M. Rooth, A. Johansson, K. Kukli, J. Aarik, M. Boman and A. Harsta, *Chemical Vapor Deposition* **2008**, *14*, 67-70.

[95] X. Y. Chen, E. Pomerantseva, K. Gregorczyk, R. Ghodssi and G. Rubloff, *Rsc Advances* **2013**, *3*, 4294-4302.

[96] M. Putkonen, T. Aaltonen, M. Alnes, T. Sajavaara, O. Nilsen and H. Fjellvag, *Journal of Materials Chemistry* **2009**, *19*, 8767-8771.

[97] O. Nilsen, V. Miikkulainen, K. B. Gandrud, E. Østreng, A. Ruud and H. Fjellvåg, *physica status solidi (a)* **2013**.

[98] J. Lee, A. Urban, X. Li, D. Su, G. Hautier and G. Ceder, *Science* **2014**, *343*, 519-522.

[99] M. Sathiya, A. S. Prakash, K. Ramesha, J. M. Tarascon and A. K. Shukla, *Journal of the American Chemical Society* **2011**, *133*, 16291-16299.

# 9 List of Papers

**Paper I:** "High-Performing Iron Phosphate for Enhanced Lithium Ion Solid State Batteries as Grown by Atomic Layer Deposition"
K. B. Gandrud, A. Pettersen, O. Nilsen, H. Fjellvåg, *J. Mater. Chem. A*, 2013, **1**, 9054.

**Paper II:** "Deposition of lithium containing iron phosphate by atomic layer deposition"
K. B. Gandrud, A. Pettersen, O. Nilsen, H. Fjellvåg, manuscript.

**Paper III:** "Surprising Rapid Intercalation Pseudocapacitance Effects in Amorphous $LiFePO_4$"
K. B. Gandrud, O. Nilsen, H. Fjellvåg, submitted (2014).

**Paper IV:** "High Power Nano-Structured $V_2O_5$ Thin Film Cathodes by Atomic Layer Deposition"
E. Østreng, K. B. Gandrud, O. Nilsen, H. Fjellvåg, submitted (2014)

**Paper V:** "Atomic layer deposition of functional films for Li-ion microbatteries"
O. Nilsen, V. Miikkulainen, K. B. Gandrud, E. Østreng, A. Ruud, H. Fjellvåg, *Phys. Status Solidi A,* 2014, **211**, No. 2

# I

II

III

# IV